Chair of Petroleum and Geothermal Energy Recovery

Master's Thesis

ESP Testing Facility Digital Twin

Jochen Peroutka, BSc

May 2022

MONTANUNIVERSITÄT LEOBEN
www.unileoben.ac.at

EIDESSTATTLICHE ERKLÄRUNG

Ich erkläre an Eides statt, dass ich diese Arbeit selbständig verfasst, andere als die angegebenen Quellen und Hilfsmittel nicht benutzt, und mich auch sonst keiner unerlaubten Hilfsmittel bedient habe.

Ich erkläre, dass ich die Richtlinien des Senats der Montanuniversität Leoben zu "Gute wissenschaftliche Praxis" gelesen, verstanden und befolgt habe.

Weiters erkläre ich, dass die elektronische und gedruckte Version der eingereichten wissenschaftlichen Abschlussarbeit formal und inhaltlich identisch sind.

Datum 12.05.2022

Unterschrift Verfasser/in
Jochen Peroutka

Jochen Peroutka, BSc.

Master Thesis 2022

Petroleum Engineering

ESP Testing Facility Digital Twin

Supervisor: Dipl.-Ing. Dr.mont. Rudolf Fruhwirth

Chair of Petroleum and Geothermal Energy Recovery

dpe

MONTAN UNIVERSITÄT LEOBEN

Acknowledgements

I am very grateful to my supervisor, Dipl.-Ing. Dr.mont. Rudolf Fruhwirth, for his patience, guidance, and continued support throughout my thesis.

I would like to extend my thanks to Dipl.-Ing. Dipl.-Ing. Dr.mont. Clemens Langbauer for his valuable suggestions and advice.

Special thanks to Ing. Andreas Öfler for his technical guidance at the Pump Test Facility Leoben.

Lastly, I'd like to thank my family, foremost my parents Gerlinde and Roderich for their continued support, encouragement, and motivation throughout my studies, my brother Martin who always helped me find a solution, and my brother Jörg with whom I accomplished this journey.

Abstract

The ever-rising demand for energy requires the oil and gas industry to expand its operating procedures with new technologies not only to increase production efficiency and profitability but also to meet regulatory compliances and increasing requirements in health, safety, and environment. Several new technologies have emerged over the last years with one of them being very promising, the Digital Twin. A Digital Twin is a virtual representation designed to simulate and mirror a physical entity. As such, new operating procedures, the implementation of additional components, and variations in the workflow can be simulated without altering an already existing production system. Several different scenarios can be evaluated with a Digital Twin with the most promising one to be implemented while reducing costs since actual field tests are not required to be conducted anymore.

This thesis aims to build a Digital Twin of the ESP testing facility located at the University of Leoben with the software program MATLAB Simulink. The Digital Twin consists of seven different subsystems that are based on mathematical formulations from literature covering all necessary parts required. This design offers high adjustability of parameters associated with the motor, the pump, and the hydraulic subsystem. Furthermore, it is possible to operate the Digital Twin by either setting a fixed voltage and frequency input or by utilizing a motor scalar control. In addition, the flow rate can be adjusted by two valves as part of the hydraulic subsystem.

The simulation output offers detailed information about the stator and rotor currents, the electromagnetic torque as well as the rotating speed generated by the motor, head losses originating from the hydraulic subsystem, and the flow rate produced by the pump. Model validation is conducted by comparing the simulated flow rate with the flow rate measured from the pump test facility. With results being close to the actual behavior the MATLAB Simulink model can be considered an early stage Digital Twin.

Zusammenfassung

Die ständig steigende Nachfrage nach Energie stellt hohe Anforderungen and die Öl- und Gasindustrie, sodass diese ihre Betriebsabläufe durch neue Technologien erweitern muss, um nicht nur die Produktionseffizienz und die Rentabilität zu steigern, sondern auch um die gesetzlichen Vorschriften und die zunehmenden Anforderungen in den Bereichen Gesundheit, Sicherheit und Umwelt zu erfüllen. In den letzten Jahren haben sich etliche neue Technologien etabliert, von denen eine besonders vielversprechend ist: der digitale Zwilling. Ein digitaler Zwilling ist eine virtuelle Darstellung, die eine physische Einheit simuliert und widerspiegelt. Dadurch bietet sich die Möglichkeit neue Betriebsabläufe, die Implementierung zusätzlicher Komponenten und Variationen im Arbeitsablauf zu simuliert, ohne ein bereits bestehendes Produktionssystem zu verändern. Mit einem Digitalen Zwilling können verschiedene Szenarien evaluiert und das vielversprechendste realisiert werden, bei gleichzeitiger Reduktion der Kosten, da die Notwendigkeit von Feldtests vor Ort entfällt.

Ziel dieser Arbeit ist die Erstellung eines Digitalen Zwillings der ESP-Prüfanlage an der Montanuniversität Leoben mit dem Softwareprogramm MATLAB Simulink. Der Digitale Zwilling besteht aus sieben verschiedenen Subsystemen, die auf mathematischen Formeln aus der Literatur basieren um alle notwendigen Zusammenhänge zu beschreiben. Dieses Design bietet eine hohe Einstellbarkeit der Parameter des Motors, der Pumpe und des hydraulischen Subsystems. Darüber hinaus ist es möglich, den Digitalen Zwilling entweder mit einem festgelegten Spannungs- und Frequenzeingang oder mit einer skalaren Motorsteuerung zu betreiben. Weiters kann die Durchflussmenge über zwei Ventile als Teil des hydraulischen Subsystems eingestellt werden.

Die Simulationsergebnisse liefern detaillierte Informationen über die Stator- und Rotorströme, das elektromagnetische Drehmoment sowie die vom Motor erzeugte Drehzahl, die durch das hydraulische Subsystem verursachten Druckverluste und die von der Pumpe erzeugte Fördermenge. Die Modellvalidierung erfolgt durch den Vergleich der simulierten Fördermenge mit der in der Pumpenprüfanlage gemessenen Fördermenge. Da die Ergebnisse dem tatsächlichen Verhalten sehr nahe kommen, kann das MATLAB-Simulink-Modell als ein frühes Stadium eines Digitalen Zwillings betrachtet werden.

Table of Contents

Chapter 1

Introduction

The oil and gas industry faces constantly declining production as more and more hydrocarbons get depleted. It becomes difficult to ensure an economic recovery with today's operational procedures. The aim is to optimize production as well as process workflows and to reduce the environmental footprint as a result of these operations. Especially unconventional resources perform unpredictably and lead to challenges that need to be overcome by the industry. Furthermore, strict regulations in health, safety, and the environment with regards to exploration, drilling, and production activities, as well as low oil prices over the last years, require a shift of oil and gas companies towards digitalization. The implementation of new digitalized procedures will not only reduce investment costs and improve productivity and efficiency of ongoing and new operations but will also lower risks associated with health, safety, and environment, increase revenues, and improve regulatory compliance.

Several new technologies have evolved in the last decade, providing tremendous potential for the oil and gas industry. Processing power is inexpensive, allowing these technologies to be implemented wherever they are needed to achieve benefits. Integration of contemporary advances in information and communication technologies, such as cloud computing, virtual and augmented reality, industrial internet of things, blockchain technology, and big data analytics enables cyber-physical communication and interaction. This cyber-physical integration enables the collection, effective analysis, and visualization of data to make better decisions, use the data as a basis for simulations, and optimize operations.

Due to new developments in Big Data processing, machine learning, and pattern recognition, supported by continuous advancements in computational power, Artificial Intelligence applications provide several advantages in different sectors of the oil and gas industry. Advances in the Internet of Things provide an interface through which sensors and actuators communicate and therefore allow for the transmission of Big Data. Gathered data gets

processed to reduce data dimensionality and to remove redundant information to uncover hidden patterns and important information that is encoded within them. A combination of Big Data Analytics and AI models for processing Internet of Things data enables one of the most promising new advances in digitalization, the Digital Twin. The Oil and Gas industry is now investigating how to apply Digital Twin technology as a result of the adoption of developing digital technologies. Currently, new digital technologies are implemented following a bottom-up approach which leads to an unsymmetrical implementation of technologies and prevents the industry from utilizing the full potential that comes from digitalization and Digital Twins. The oil and gas industry needs to carefully evaluate all limitations associated with these technologies. Only with a proper understanding, all benefits of Digital Twins can be utilized.

1.1 Scope and Objectives

This thesis aims to build a Digital Twin of the ESP testing facility located at the University of Leoben. The model contains all necessary components based on mathematical formulations from literature and is divided into seven different subsystems that are interconnected. The electrical supply can either be adjusted with fixed voltage and frequency or by utilizing a motor control subsystem based on the principle of scalar control. An induction motor functions as the drive unit and is simulated according to the so-called Park frame that transforms a three-phase system to an equivalent two-phase system in a rotating reference frame. Determination of the pump head curve is accomplished by utilizing a polynomial function with parameters identified after the principle of Ordinary Least Squares. Furthermore, the torque curve is simulated with a polynomial function whose input parameters are graphically estimated from the pump power curve. The hydraulic subsystem includes head losses originating from friction, height difference, velocity, and local losses due to the pipe geometry. In addition, two valves are included in this subsystem to not only control the flowrate by a set motor speed but also to offer the possibility to further adjust the flowrate with different valve settings. The simulated flow rate of the Digital Twin model is compared with the flow rate of a test run conducted at the pump test facility.

1.2 Overview of Dissertation

The second chapter covers an extensive literature review of the Digital Twin including its characteristics, different frameworks that describe enabling components upon which digital twins can be built, the classification of Digital Twins as well as the implementation of Digital Twins based on the system's complexity. Furthermore, applications of Digital Twins in the oil and gas industry are specified including various risks that might originate from such endeavors. Chapter two continues with an overview of prominent artificial lift systems, a detailed explanation of the working principle of ESPs as well as fundamental information about ESP drive units. Chapter three gives an in-depth overview of all mathematical formulations and their relationships that are necessary to realize the Digital Twin model in MATLAB Simulink. The fourth chapter covers the implementation in MATLAB Simulink and how the model is designed with graphical representations of the whole system as well as comprehensive information about all subsystems including the implementation of the mathematical formulations into MATLAB functions. Chapter five presents the output results that can be obtained from the Digital Twin model and includes a model validation with the flow rate being compared to that from the pump test facility. The sixth chapter concludes the creation of the Digital Twin and gives an outlook on future enhancements that can improve the simulation.

Chapter 2

Literature Review

2.1 Digital Twin Characteristics

Digital Twins are computer-based models or machines designed to emulate, mirror, simulate, or "twin" a physical entity. This physical entity can be related to an object, a process, a human, or a human-related aspect. Each Digital Twin is linked to its physical twin by a unique key that identifies the physical twin and thus allows the Digital Twin and its twin to form a bijective relationship. A Digital Twin is not only a simple simulation or model, but it is also a virtual representation of a living, intelligent, and evolving real entity or process. A Digital Twin constantly monitors the behavior of its physical twin. The exchange of data allows for controlling as well as optimizing operations. It continuously predicts future trends like malfunctions, damages, and failures, and enables the simulation and testing of unique configurations to perform preventive maintenance. The process of generating a Digital Twin is facilitated by constant interaction, communication, and synchronization between the digital Twin, its physical twin, and the external environment. When dealing with large amounts of data, feature extraction and selection are important. A successful real-time cyber-physical synchronization as well as enabling the so-called "closed-loop optimization" is based on successfully obtaining the most important value and information from big data exchange. Closed-loop optimization is the process of continually exchanging data between the cyber domain and physical domain to improve the physical side. All exchanged data must be saved in a data storage system that the digital twin has access to. The data storage also includes descriptive static data to describe essential twin traits as well as historical static data. Historical static data reflect the memory of the physical twin and can stock historical information either as a result of past actions or by human expertise. The objective of Digital Twins is to provide more valuable, accurate, and consistent data. This is accomplished by working with

multidimensional data sets rather than individual data sources. As a result, effective high-dimensional data coding and decoding, data fusion methods for combining numerous sources, and appropriate analytic techniques must be established. Big data storage capabilities and real-time data uploading are reasonably inexpensive nowadays which enables a frequent and constant update and exchange of descriptive data. As Digital Twins analyze frequently received sensed data from the physical twin and the local environment, DT technology incorporates supervised and unsupervised learning algorithms that improve their prediction capabilities. The Digital Twin can operate as an expert system by using descriptive, predictive, and prescriptive algorithms to carry out a sequence of procedures. A complex set of objectives, requirements, and restrictions necessitates relevant decisions to be made to generate a set of high-value alternative actions or decisions, with descriptive and predictive analytics serving as inputs to prescriptive analytics. It then employs stochastic optimization methods to find the best solution while considering data uncertainty. Due to real-time updates from its physical twin and other digital twins in the surroundings, the digital twin is always aware of what is going on in the real world. It evolves in conjunction with its physical counterpart using data fusion techniques, Big Data analytics, and AI descriptive algorithms, thanks to a modular and highly parameterized architecture that allows for quick reconfiguration. In addition to using predictive and prescriptive algorithms, the DT uses proper ontologies and high-dimensional data-coding techniques to describe the derived prescriptions and optimization schemes. This permits feedback to be sent to both the physical twin and other DTs. End users, on the other hand, can employ interaction interfaces to retrieve computed data and evaluate the DT status. The DT also incorporates modeling and simulation tools for depicting the physical twin's current state as well as future potential realistically and naturally. In addition to this extensive emulation, the DT's AI allows finding information such as system descriptions, hidden patterns, and unknown correlations. The capability to record, control, and monitor the physical system's states and changes enable AI predictive and prescriptive approaches to be used for forecasting failures, evaluating the success of potential remedies, and triggering self-healing mechanisms. This leads to the so-called predictive maintenance strategy, in which malfunctions are foreseen and fixes and/or alterations are simulated to avoid mistakes or identify the best solutions. [1, pp. 104175, 104176, 104178, 2, pp. 108952, 108953]

2.2 Framework

Although there are several different frameworks developed for digital twins, the most widely accepted framework consists of three fundamental components, the physical domain, the virtual domain, and a connection between these two. The physical asset, actuators, and sensors are part of the physical domain, while multi-physics, multi-scale and probabilistic simulation models

gather and analyze data and perform simulations to find the optimal control parameters and conditions for the physical asset are in the virtual domain. A connection between the real and virtual domains enables the possibility to transfer data and actuation commands seamlessly between them. The DT is thus continually synced with its physical counterpart and changes in lockstep with it, with the change reflecting and being dictated by the attributes of the reflected physical object.

An alternative to the three-component framework of a Digital Twin is the five-component framework that is comprised of physical space, virtual space, and Digital Twin data fusion model as well as different service systems with a connection/ interaction between these four modules acting as the fifth component in the system. The digital counterpart for high-fidelity simulation of the physical equivalent in the virtual space. The service system consists of several parts. These are data services, algorithm services, model calibration services, diagnostic services, visualization services as well as product quality services. The connection between the virtual and physical world as well as the service systems is provided by the data fusion model of the Digital Twin. This data fusion model combines and analyzes the acquired data to provide driving commands for the other three modules by gathering information from sensors (the physical space), the simulation (the virtual space), and the service systems.

Deloitte provides an enhanced digital twin framework that is built upon five enabling components and a six-step process. These five components include sensors, data, integration, analytics, and actuators. Sensors and actuators are located in the physical space, while data analytics occurs in the virtual space. Integration technologies must be applied to enable seamless data and command transmission between the physical and virtual (digital) worlds. Edge processing transforms proprietary data protocols into more comprehensible data formats. Edge security provides the necessary security protocols and encryption to protect the DT and sensor data against cyber-attacks, while communication interfaces serve as an intermediate between sensor functions and integration functions. The digital twin-based operations are divided into six iterative steps with act, create and communicate as part of the digital domain and aggregate, analyze, and insight as part of the physical domain. Operational and environmental conditions of the asset are recorded by sensors attached to the physical domain to create electrical signals. Real-time data from the physical world is corporated in conjunction with other data such as event logs, engineering datasheets, design specifications, engineering drawings, and material lists. Tools such as augmented and virtual reality, big data analytics, and machine learning in combination with advanced analytics allow for proper processing and visualization of collected data. If actions on the physical asset are necessary, the Digital Twin provides them and applies those to the system's actuators. Digital Twins are intelligent systems but they may not always be fully autonomous as the implementation may be subject to human

intervention. In scenarios where AI-based applications and digital twins are used to test new features and alterations of physical assets, or when they are utilized to provide answers such as diagnosis and treatments human intelligence is not necessarily more efficient than DT's AI; nevertheless, human capabilities enhanced by DT's analysis, predictions, and prescriptions are unquestionably more productive. [1, pp. 104178,104179]

2.3 Classification

The two main categories in which Digital Twins can be classified are plant twins and process twins. While the plant twin is a three-dimensional model in the digital or physical realm and serves as a smart viewer and advanced simulation platform, the process twins' task is to investigate an asset’s behavior and performance, and functions as a digital representation of an automation system or process.

Access to engineering, operations, maintenance, and asset performance data enables Plant twins to execute various scenarios of future operational outcomes, known as what-if scenarios, which aid the operator in planning future endeavors such as construction, operation, maintenance, repair, commissioning, and decommissioning activities. The plant twin may also be used to evaluate engineering, procurement, and construction plans, allowing for the early detection of design flaws and necessary adjustments, saving capital expenditure for late-stage modifications. Furthermore, the plant twin may be utilized to conduct immersive virtual training that takes field personnel through field operations and maintenance tasks, as well as emergency evacuation training. Training programs allow field personnel to traverse the plant twin using a virtual avatar or virtual/mixed reality-based devices that provide the perception that the employees are operating in a real plant.

Process twins are digital representations of processes and automation systems. This allows identifying the best operation parameters and conditions as well as associated safety protocols. Engineers can then run a series of simulations to test new operating processes, maintenance schedules as well as emergency response processes. Additionally, the results can be facilitated to tune controllers and test instrumentations or control and safety installations. Like plant twins, process twins also enable the possibility for personnel training that allows operators to gain experience from various operating setups and process scenarios requiring them to respond accordingly to these scenarios and conditions.

Siemens, a global leader in digitization, expands the two types of Digital Twin classification and introduces a third level based on key functionalities, where the levels represent fundamental differences in the level of detail and accuracy requirements. These three levels in which Digital Twins are classified are equipment-level, system-level, and plant-level. The equipment level

twin contains comprehensive engineering drawings, engineering designs, as well as production and engineering data. The equipment level twin should maintain precise engineering, manufacturing, and design data, that is updated and maintained over the equipment's life cycle assisted by utilizing product life cycle management software. The equipment-level twins are then combined into a single unit to create a system-level twin. Generally, the system-level twin is inaccurate in terms of the engineering, manufacturing, and design data related to the entire equipment, however, it gives a realistic depiction of the aggregated operation of all of the system's equipment. These system-level twins are then subsequently merged to form the plant-level twin that intends to duplicate the overall plant performance. [1, pp. 104179, 104180]

2.4 Enabling Technologies and Sample Systems

The successful implementation of digital twins depends on the connection between the digital twin and the physical asset. Enabling technologies need to properly utilize this connection to allow for data acquisition. Gathered data is evaluated either directly at the sensor or transmitted to a data warehouse where it gets processed further to uncover hidden patterns and additional meaningful insights. Technologies such as 3D/4D modeling and CAD; supervisory control and data acquisition and other smart sensors; big data, data analytics, and data warehouses; machine learning, deep learning, and artificial intelligence; virtual systems, environments, and models; virtual reality and augmented reality; web and cloud-enabled technologies; automation; wireless sensor networks and location trackers; as well as high-performance computing enable the acquisition, transfer, storage, analysis and visualization of data gathered by digital twins to improve operations by increasing safety, productivity, and revenue. [1, pp. 104180]

2.5 Implementation

Proper implementation of Digital Twins is mostly driven by the system's complexity and to adequately represent that complexity. The Twin model should neither be overly simplistic since this leads to a loss of value that the Digital Twin typically provides, nor should it be overly complicated, with millions of sensors, hundreds of millions of sensor data, and complex technologies necessary to extract value from these data. An approach for the proper implementation of Digital Twins consists of six steps and is shown in Figure 1.

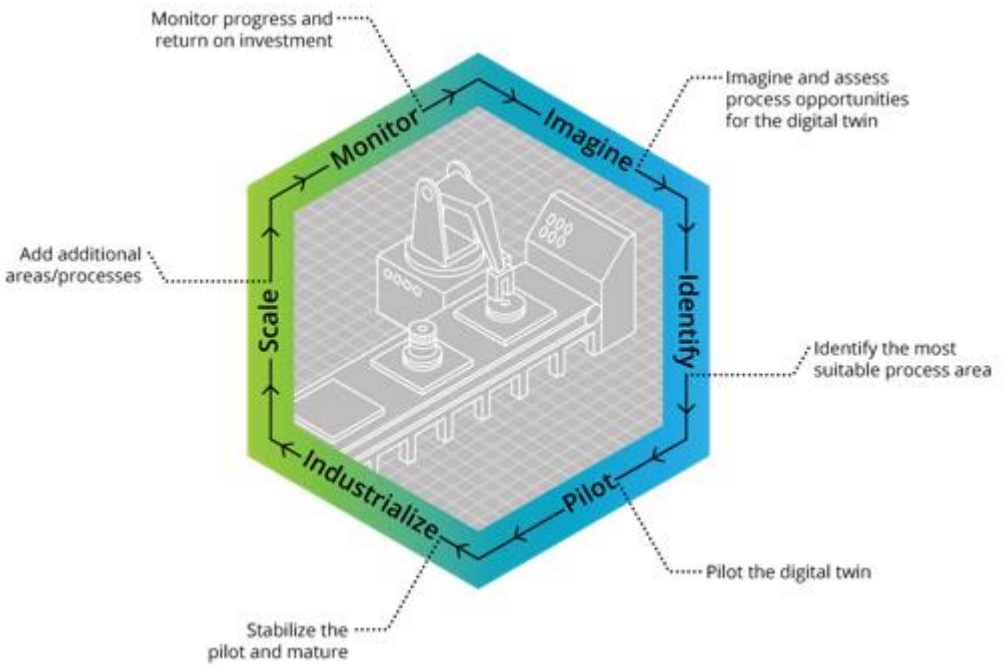

Figure 1: Digital Twin Implementation [1, pp. 104180]

The first stage is to imagine the possibilities if any scenarios benefit from a Digital Twin. Depending on the organization and various circumstances this might differ from one to another but two key aspects might always be taken into account. It must be clearly stated if the enterprise gains enough value by investing in a digital twin for the product or manufacturing process and if it is possible to uncover value for consumers or the company from an unresolved, unexplained process or product issues. In the next part of the identification process members of the business, operational, and technical leadership asses the given scenarios and decide which parts of the process of implementing a digital twin lead to quick wins. The second stage identifies the mechanism through which the digital twin configuration, taking into account operational, organizational, and business change management aspects, leads to the highest possible value gained from executing the pilot twin and the best likelihood of success.

The main problem could be that the digital twin is not implemented across the company but rather focuses too strongly on a specific piece of equipment, technology, or site. Therefore, digital twins with a wide range of applications provide more value and support for a given endeavor.

The third stage focuses on the fast implementation of a pilot program with an open and agnostic ecosystem that allows for adaptability and integration with new structured or unstructured data to expedite learning, maximize return on initial investment, and manage risk proactively. In this stage, scope limitation is important, while the twin still needs to maintain the ability to provide value for the organization.

If the digital twin is successful, stage four proposes to industrialize the digital twin development and deployment. This is achieved by using established tools, strategies, and playbooks while managing expectations from the pilot team as well as other projects interested in adopting it.

The goal to support the digital twin is to move from a more siloed approach to enterprise integration by introducing a data lake, enhancing efficiency and throughput, improving data governance and data standards, and implementing organizational adjustments.

Once the preceding phases have been completed successfully, lessons learned from the pilot twin should be utilized to identify opportunities that can scale the digital twin. Adjacent processes or activities that are connected with the pilot twin are utilized and the value gained from such an endeavor as a result of the digital twin adoption should constantly be conveyed. In the final step, the digital twin should be constantly monitored and measured to iteratively adjust the digital twin to find the best possible configuration. It is important that if a suitable configuration is identified, new cycles should be conducted to continuously increase delivered benefits. [1, pp. 104180]

2.6 Opportunities and Applications

2.6.1 Asset Performance Management

Digital Twins collect data in real-time from assets such as oil and gas facilities as well as components deployed in these facilities. The acquired data range from production rates, bottlenecks in the system, operational conditions and malfunctions as well as potential failure modes and rates, control parameters for production optimization, to structural integrity level of assets, and requirements for maintenance and replacement. Data then gets processed and potential risks and key performance indicators are visualized to optimize asset operation in terms of production, interventions for repair and replacement, perform scenarios with various conditions to evaluate the most promising production schedule, and identify de-rated operating conditions that might have structural integrity issues. Optimized repair and maintenance strategies help to avoid unplanned interventions. In addition, the asset lifespan can be increased by circumventing frequent asset shutdowns and restarts without increasing HSE risks. In addition to improving the performance of existing assets, data from a digital twin can be saved in data management systems and utilized as a reference to improve the development of new projects. [1, pp. 104185,104186]

2.6.2 Asset Risk Management

Oil and gas facilities usually deliver large quantities of data that cannot be analyzed by human operators. Digital twins, on the other hand, have big data analytics capabilities that allow them

to process large amounts of data utilizing machine learning, deep learning, and artificial intelligence algorithms. The digital twin continuously monitors the parameters of all assets to identify potential risks and failures and delivers alerts to responsible parties such as operators and regulatory bodies to avoid any incidents. New operating methods and equipment are tested and evaluated if they pose any harm or risk to the facility, environment, or people. Once a safe operation of the tested assets and procedures is ensured, the new parameters are implemented to the physical asset to comply with HSE standards and regulations. [1, pp. 104186]

2.6.3 Virtual Training to Navigate and Operate

In the near future over 50 percent of experienced employees in the oil and gas industry will retire. This leads to a severe lack of skilled personnel. Because the knowledge and skills of these senior experts may not be adequately transferred to new personnel, training programs must be created to ensure that oil and gas facilities operate as efficiently as possible. Digital twins can be operated in conjunction with technologies that extend the reality such as virtual and augmented reality. This allows new personnel to navigate within such a setup and to monitor, operate, and inspect systems in this virtual environment. This type of program helps new employees to become familiar with particular operational procedures while also lowering the risks associated with training on a physical asset in the real world. [1, pp. 104186]

2.6.4 Emergency Response Training

Regularly scheduled safety training is mandatory for the oil and gas industry. Such training often results in loss of production since related equipment needs to be shut down meanwhile. Offshore training, in particular, is not only expensive in terms of lost production and equipment fatigue due to shutdowns, but it also exposes personnel to unnecessary risks as a result of such training. A digital twin of such a facility allows personnel to be trained in a virtual environment without the constraints that come with on-site training on the physical asset. [1, pp. 104186]

2.6.5 Shorter Time for Plan to Production

Typically, the design and planning of an oil and gas facility incorporates numerous steps to completion resulting in a relatively long endeavor. Offshore platforms, in particular, have a unique design depending on reservoir characterization and field location, necessitating engineers to design such platforms from scratch, extending the time to production. With the implementation of digital twins in such a program, experts can use models from prior platforms as a starting point, alter specific characteristics based on the requirements, and execute numerous test runs on this virtual facility. Design data and various components from vendors are tested until a safe and optimized facility design is approved, resulting in a significantly

shorter time to production. Once the design process is completed, the facility needs to go through a commissioning phase, which takes time and also poses HSE risks. With the use of high fidelity digital twins, facility parameters can be pre-tuned and control loops verified for proper operation prior to production, all while saving time and lowering HSE risks. [1, pp. 104186, 104187]

2.6.6 Avoid Miscommunication and Information Wastage

Miscommunication and information waste are the two most damaging components of supply chain tracking and project documentation. If a piece of equipment is changed during the design stage of an oil platform, for example, not all parties involved are aware of the change. That equipment may not fit once construction begins, resulting in a construction delay. A communication failure like this may be prevented by updating the digital twin, which will then notify all relevant parties by email and message, or by raising an alarm until the changes are recognized by the relevant providers. [1, pp. 104187]

2.6.7 Collaborative Decision making

Due to the fact that the oil and gas industry is very capital intensive, any unplanned downtime causes considerable production and revenue losses, as well as increased HSE risks. When equipment breaks, usually several experts are involved in the process to cooperate and investigate possible solutions, however, these specialists may not be on-site or co-located, and must rely on telecommunication. This strategy may pose issues due to its limited effectiveness. Digital twins facilitate cooperation by giving experts insight into critical facility data, discussing challenges, and finding solutions regardless of their location. Virtual control rooms can also be implemented to simulate and decide the best solutions for a specific situation and therefore increasing collaboration effectiveness even more. [1, pp. 104187]

2.6.8 Process Automation

Digital twins are connected to their physical assets and constantly record sensor data. This sensor data is analyzed and processed in real-time. To increase the operation consistency as well as avoid any interruptions, the digital twin can determine new control schemes for actuators and related equipment. Furthermore, digital twins can be used to automate processes on drilling rigs, production facilities, or process facilities. Automation offers the possibility to remove human workers from dangerous or hazardous areas. Without the involvement of human workers, the accident rates can be reduced, and the safety of the facility improved since most accidents have some element of human error. [1, pp. 104187, 104188]

2.6.9 Future Scenario Development

With a digital twin of an oil and gas asset, it is possible to alter assets with new components or changed process parameters. With such an implementation the nonproductive time of the real asset can be reduced since test runs are conducted on the digital twin. Once the evaluation of such what-if scenarios is finished the newly obtained optimized process parameters and components can be installed. [1, pp. 104188]

2.6.10 Effective Time Utilization

Sensors at oil and gas facilities usually produce large volumes of data that must be reviewed, processed, and analyzed in order to detect essential operating conditions, assure asset reliability, maintain regulatory compliance, and address safety and critical process concerns. This data procedure, on the other hand, is time-consuming and necessitates a workforce that could otherwise be employed for different duties. If the data is gathered and processed by digital twins personnel may focus on implementing the digital twins' outputs to enhance the process safety, increase production and revenue, and satisfy regulatory requirements rather than spending time assessing and processing data by hand. [1, pp. 104188]

2.7 Challenges

The oil and gas business is confronted with numerous challenges as a result of the adoption of digital twins, all of which must be fully recognized and addressed in order to prevent any risks that may arise. Existing company models and operations are substantially altered, necessitating adequate employee adaption. Another issue is that different forms of data acquisition provide various types of data such as structured, unstructured, and semi-structured data, making it difficult to merge them into a single database. Cyber attacks can compromise the relationship between the physical asset and its digital duplicate, necessitating a high level of protection in the form of advanced cyber security protocols as well as industry-wide standards and regulations. Furthermore, data ownership must be clearly stated in terms of which parties involved have access to digital twin data and who is permitted to alter them. [1, pp. 104188-104190]

2.7.1 Scope and Focus

Before the implementation of a digital twin, it must be clearly stated in which areas of process and what types of assets it will represent. New technologies such as the industrial internet of things, smart sensors, virtual and augmented reality, machine learning, deep learning, and artificial intelligence facilitate the development of highly complex digital twins that can resemble every aspect of a facility while also delivering large amounts of sensor data that must

be addressed properly. The user may become overwhelmed by the ever-increasing quantity of sensor outputs and digital technologies available. On the other hand, a digital twin with an overly simplistic design may not be possible to deliver adequate information about the physical asset necessitating the use of several digital twins to overcome limitations. [1, pp. 104188]

2.7.2 Lack of Standardization

Sensors in the oil and gas industry deliver huge amounts of data that do not often follow a data standard. Data formats can be unstructured like portable document formats, semi-structured such as log files from integrity management programs, or structured like excel spreadsheets. Additionally, data from suppliers may also follow different standards. Once data is gathered they are stored, however, different data standards lead to complications in storing these data in a centralized database. Often data gets stored in several siloed compartments which makes it difficult for the digital twin to access them. Since the success of a digital twin depend on how well it can understand and process data and produce meaningful results, the oil and gas industry already works on solutions regarding different data standards. [1, pp. 104188]

2.7.3 Cyber Security

A cyber-physical interface connects a digital twin to its physical counterpart. This interface allows the digital twin to not only collect data, but also analyze it in real-time, allowing it to analyze asset performance, produce new control schemes as needed, and offer extra operating strategies. Hackers can take advantage of the cyber-physical link, making the digital twin and its real asset vulnerable to cyber assaults that can result in catastrophic failures. Exploration, development, production, and abandonment are the three main stages of an oil and gas field.

Exploration contains operations such as seismic imaging and geological and geophysical surveys which have a closed data acquisition since most of the data from rock formations are captured by geophones, magnetics, or hydrophones and transmitted by physical interphase. This makes exploration less vulnerable compared to other stages, however, exploratory and appraisal drilling does have a higher risk profile. From a financial risk point of view cyberattacks against exploration are less harmful in terms of business disruptions as well as for health, safety, and environment. The most critical part is a company’s field data, and cyber-attacks might eventually not be noticed right away due to no direct costs or visible impacts.

Within all stages of the oil and gas value chain, development is most vulnerable to cyber-attacks. It entails comparable operations to exploratory and appraisal drilling, but there is greater potential for cyber attacks due to more regular drilling activities, equipment deployed on the surface and below, as well as diverse partners and consultants that may not share the same cybersecurity protocols. Due to higher drilling activities and new advances in real-time

remote control of drilling operations, hackers may readily get access to sensitive drilling data. Development drilling does not only have the highest vulnerability to cyber attacks out of all development operations, but cyber attacks can also lead to devastating outcomes resulting in business disruptions, reputation damage, health, safety, and environmental risks, or even the loss of an asset. The other two development phases, field development, and well completion have a relatively lower risk profile.

The production stage is most vulnerable to cyberattacks due to its legacy assets that are simply not built for cybersecurity. This means that only a few of such legacy assets have properly operating security monitoring systems. This problem originates from the expansive operating environment which includes a diverse set of control equipment from different vendors which follow different cyber security protocols. In addition, such control systems are more and more linked to the enterprise resource planning systems of the company. Production data like pressure, flow rate, or density are more likely to be understood by hackers compared to data from seismic and drilling operations. This can lead to severe dangers if hackers have the possibility to alter them. Well intervention, workover, and abandonment are less vulnerable to cyber-attacks compared to production since these processes mostly include mechanical alterations, well diagnostics, and maintenance, however, vendors increasingly add software solutions and interfaces to reduce costs that can result in a higher vulnerability risk.

The oil and gas industry has to pay more attention to cyber criminality and the severity of such assaults in order to avoid or at least limit any hazards that may arise. With the right countermeasures in the form of advanced cyber security protocols, oil and gas companies should be able to protect their virtual and physical assets. [1, pp. 104188, 3, pp. 10-14]

2.7.4 Data Ownership and Sharing

Digital twins generate all sorts of data that can be beneficial in various ways. Since data will play a key role in the future of the oil and gas industry on their way to becoming more digitalized, digital twin’s data can be used to design new and improved assets and for developing new data science algorithms. As there are many different parties engaged in developing a digital twin and utilizing its output to increase efficiency, it must be specified which parties involved do have what rights in terms of data ownership. Protecting intellectual property rights, enabling secure access for relevant parties, distributing duties, and defining the amount of access that specific stakeholders may have are the most important tasks. [1, pp. 104189]

2.7.5 Accuracy and Validity

A digital twin has to be as accurate as possible compared to its physical asset in order to derive valuable insights. Normally digital twins produce several models. While some parts are based on the underlying physical principle, other parts of the digital twin are derived empirically from machine learning methods. To accurately replicate the physical behavior it is essential to properly tune the model, however, such tuning might be a complicated task. The goal is to reduce any deviation between the results produced by the digital twin and the measured data from the physical asset. Differences in outputs originate from defective sensors, not properly working physical assets, or faults in the model itself. [1, pp. 104189]

2.7.6 Functionality

Digital twins generate vast amounts of data, however, redundant information must be filtered so that the oil and gas company employees are not distracted. Therefore, digital twin designers need to collaborate and understand the principles of the oil and gas business to properly tune and design their digital twins not only to allow operators to customize data but also to ensure they can individually select valuable information while reducing distractions caused by excessive data. [1, pp. 104189]

2.7.7 Unlocking Experience

The oil and gas industry gathers data and implements simulations for a long time. Until now, human specialists have assessed and evaluated these data and simulations. These human experts have a thorough understanding of the oil and gas industry's continuous operations, and they utilize that expertise to analyze oilfield data, spot abnormalities, and assess their causes. Usually, this information is held in someone's memory or complicated data management systems, making it difficult to access it, as well as various concepts and solutions for the implementation of digital twins. [1, pp. 104189]

2.7.8 Business Model, People, and Policies

With the digital twin implementation, several preparations need to be conducted to ensure seamless interaction between the digital twin and its operator. Permission to data access needs to be determined, new policies must be provided to prevent any data breaches, and legislative frameworks to safeguard intellectual property rights must be implemented. These precautions are important to secure the digital twin and its physical asset, nevertheless, with such a tight structure in place, the installation of digital twins may face employee resistance. Employees may not appreciate how digital twins change already established working principles. To be accepted, digital twins must deliver quantifiable benefits, unfortunately, implementing a digital

twin that can do everything is not feasible. If a digital twin can only be utilized in a certain area of interest, employees who do not profit from a digital twin may reject its implementation. Another issue is the link between digital and physical assets, which is subject to cyber-attacks and may lead experts to oppose deployment. Employees must be appropriately educated about the benefits of digital twins, improved cyber security standards must be implemented, and strategies developed to enable a flawless digital twin adoption. [1, pp. 104189, 104190]

2.7.9 Data Storage and Analytics

Sensors linked to oil and gas assets provide a tremendous quantity of data. Typically, these data contain systematic or unsystematic noise, which must be filtered before being used in machine learning simulations. Furthermore, a comprehensive data warehouse must be established for data storage and be protected against cyber-attacks, as well as easy data accessibility to assure quick availability when needed. However, user identification protocols are necessary to be installed to only permit access to people that are authorized. Additional challenges for the implementation of machine learning algorithms in the field of data analytics emphasize questions upon deciding if the analysis should be performed in batch, semi-batch, or real-time, which type of machine learning model should be implemented, and whether data warehouses are implemented a cloud-based type or a type of on-premise, which requires an additional third party involved. [1, pp. 104190]

2.7.10 Maintenance

Regularly scheduled maintenance is not only important for any physical asset but also digital twins need to be examined to ensure that they are ready for new projects. During their life cycle, digital twins go through several phases. This starts with exploration to appraisal, over development and production, and results in abandoning. During all of these live cycles, constant monitoring and recording of data are necessary requiring complex software tools, the appropriate hardware infrastructure as well as sensors attached to the asset. Therefore, a multidisciplinary project group trained to conduct digital twin maintenance needs to be recruited while also considering the costs associated and benefits gained from such an endeavor. [1, pp. 104190]

2.7.11 Incremental versus Disruptive

Oil and gas companies start investing in new digital technologies to increase revenue while also reducing risks associated with HSE. However, many of these companies follow an incremental approach, meaning that only small parts are adopted to digitalization and this results in lost value in terms of operational capabilities. The goal is to follow a disruptive approach that

changes already existing patterns in such a way that digitalization can be fully embraced and to lower the risks that the implementation of a digital twin only leads to marginal or even no benefits to operations. [1, pp. 104190]

2.8 Artificial Lift Methods

Early-stage oil wells have adequate pressure at the bottom of the well to compensate for pressure losses along the flow path to the separator. These wells are known as flowing wells, and oil can be produced to the surface without the need for artificial lifting methods. If the bottom hole pressure falls below a certain level, the natural flow of oil to the surface stops, and the well dies. The other possibility is that the pressure losses along the flow path increase as the well's flow resistance increases either because the density of the oil increases as more and more gas gets depleted from the reservoir or certain mechanical changes such as a change in tubing size to a smaller diameter or other restrictions downhole occur.

Once such restrictions occur it is necessary to install artificial lift methods to either enable the production of wells that stopped flowing naturally or to increase the production of flowing wells. Artificial lift methods can be grouped based on their underlying principle in methods that use some kind of a pump placed beneath the liquid level to artificially increase the pressure of the well stream and overcome pressure losses along the flow path, and in methods that utilize compressed gas that is injected from the surface into the tubing to lower the density of the fluid and enable fluid flow to the surface. [4, pp. 1]

2.8.1 Gas Lifting

Gas lifting employs a high-pressure gas, commonly natural gas, although other types like N2 or CO2 are also viable possibilities, and this high-pressure gas is injected into the well stream at a certain position downhole.

In a continuous-flow gas lift, the gas is injected at a constant rate into the tubing, and pressure losses along the flow route are decreased by aerating the liquid, resulting in a reduction in flow resistance. As a result, the initial bottom hole pressure is adequate to convey the gas-liquid mixture to the surface, allowing the well to flow.

Another option of gas lifting is an intermittent gas lift where the gas is not injected continuously but periodically into the tubing. When a sufficient enough liquid column has accumulated at the bottom of the well a large volume of gas is injected below the liquid to transport it to the surface in form of slug production. Once the wellbore is cleaned gas injection is stopped and a new cycle begins by letting a column of liquid accumulate at the bottom of the wellbore.

A plunger lift is a variation of the intermittent gas lift where a plunger is placed beneath the liquid column. The plunger can travel in the tubing and functions as a barrier between the liquid column and the injected gas while it is pressed by the injected gas upwards and moves the liquid to the surface. [4, pp. 1,2]

2.8.2 Pumping

Pumping utilizes a pump that is placed downhole to overcome the pressure losses along the wellbore by increasing the wellbore pressure. Generally, pumping can be classified into two categories depending on how the pump is driven downhole.

Pumps in the first category employ a string to connect the downhole pump to a driving mechanism at the surface and depending on which type of pump is used the movement refers either to rotation or oscillation. Walking-beam pumping, also known as sucker rod pumping, is the most common type that falls in the category of positive displacement pumps. Sucker rod pumps however are unfeasible for deep well production, necessitating the deployment of more suitable drive systems such as pneumatic drive or mechanical drive long-stroke pumping. One such pump that can be utilized in deep wells is the so-called progressive cavity pump. This pump is also based on the principle of positive displacement such as sucker rod pumps, but in comparison does function without any valves installed.

Instead of using rods to link the downhole pump to a surface drive unit, rodless pumping uses a driving mechanism such as electric or hydraulic devices. Rodless pumps come in a variety of styles, including centrifugal, positive displacement, and hydraulic. Hydraulic pumps are powered by a downhole hydraulic engine that rotates in an alternating motion to run the pump. The turbine-driven pump employs a multistage centrifugal pump section as well as a multistage turbine in series. The turbine is supplied with a high-pressure power fluid from a surface unit and the power fluid drives the centrifugal part of the pump at high speed to lift well fluids to the surface. Jet pumping also utilizes a hydraulic fluid by converting a high-velocity jet stream into work to deliver well fluids to the surface but differs from other hydraulic solutions in that it does not have any moving parts installed. Electric submersible pumping uses an electric motor that drives the multistage centrifugal pump and is powered by a cable from the surface. [4, pp. 2,3]

2.8.3 Comparison of Lift Methods

Besides the aforementioned artificial lift methods, there are also other methods available but their importance is negligible. Figure 2 published by the Artificial Lift Research and Development Council shows the number of different artificial lift systems installed as well as the production share.

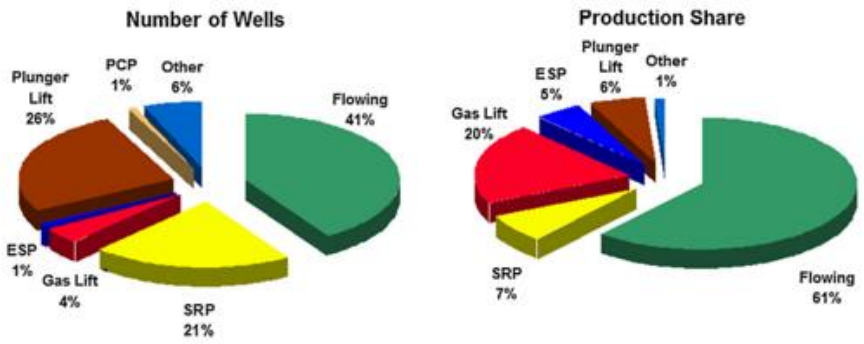

Figure 2: Oil Well Installations and Production Share [5, pp. 4]

Since there is a variety of such installations available it is important to select a proper lifting method tailored to the specific needs of each well. Limiting parameters such as well depth, desired production rates, and/or fluid properties narrow the feasible lifting mechanisms but usually there is more than one method suitable that requires engineers to select the most profitable solution in terms of production. [4, pp. 3]

2.8.4 Lifting Capacities

Artificial lift methods can be compared by their production rates associated with the corresponding depth. Gas lifting provides the highest liquid rates over the largest depth interval, followed by electrical submersible pumps and jet pumping as shown in Figure 3.

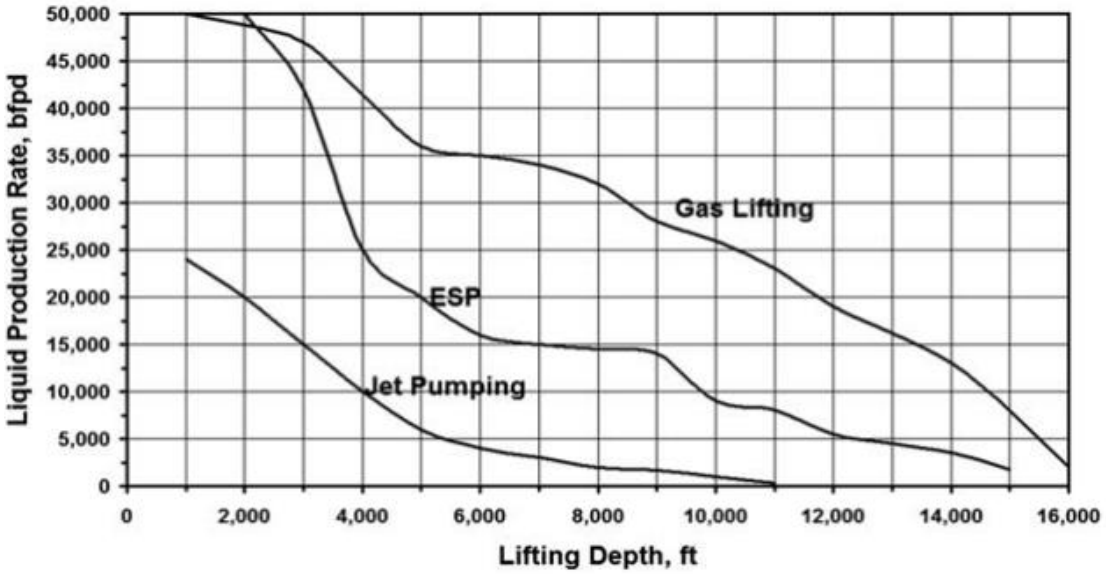

Figure 3: Liquid Production Rates versus Lifting Depth for High-Rate Artificial Lift Methods [4, pp. 4]

Hydraulic pumping, progressive cavity pumps, sucker rod pumping, and plunger lift provide significantly lower production rates compared to the lifting methods shown in Figure 3. The

liquid production rates over the lifting depth of these moderate capacity lifting methods are shown in Figure 4.

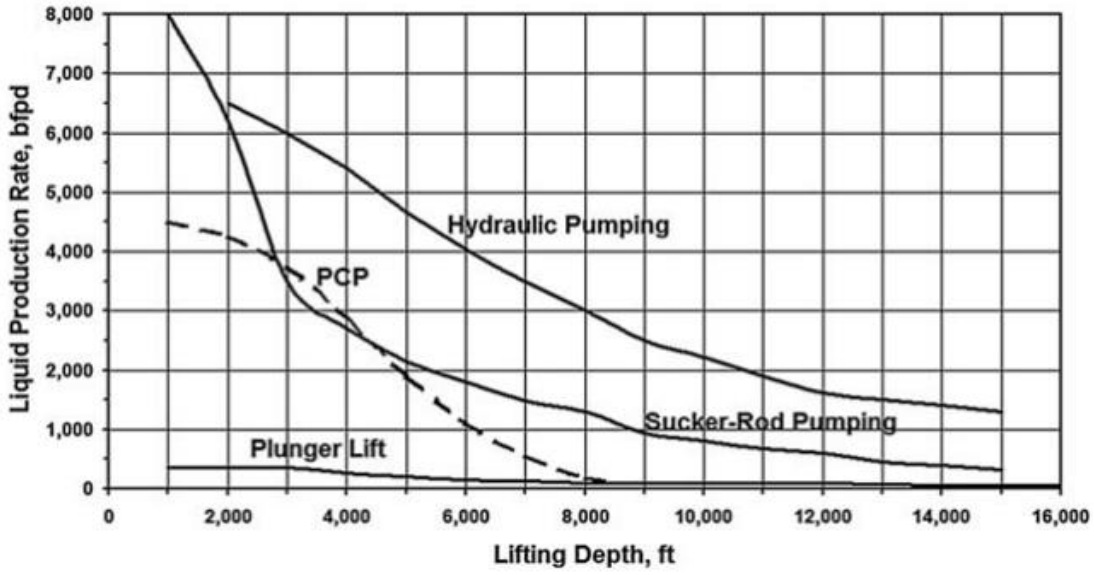

Figure 4: Liquid Production Rates versus Lifting Depth for Moderate Capacity Artificial Lift Methods [4, pp. 4]

Overall it can be stated that for all artificial lift methods presented the lifting depth has a tremendous impact on the lifting capacities meaning that the well rates rapidly decrease with increasing depth. [4, pp. 3-5]

2.8.5 Energy Efficiency

Energy efficiency is very important in the oil and gas industry and depends on the total energy required to operate the pump as well as the energy spent to lift the fluids to the surface while the efficiency results from the product of these two energy components. As shown in Figure 5, progressive cavity pumps are the most energy-efficient artificial lift methods available. These pumps achieve efficiencies up to 70 [%] by converting mechanical power provided from the surface motor to hydraulic work required for lifting the fluids. In addition, progressive cavity pumps benefit from the relatively simple surface and downhole installations, resulting in a fast-growing number of applications wherever certain parameters for proper usage are met.

With a maximum energy efficiency of around 60 [%], sucker rod pumps and electrical submersible pumps are just below progressive cavity pumps. However, these pumps suffer from high downhole losses due to their power transmission as well as drastically reduced hydraulic output when producing free gas resulting in losses of the overall system efficiency. Hydraulic pumping units that utilize positive displacement pumps have mediocre energy efficiencies of around 50%. At the bottom of the line are jet pumping devices as well as continuous flow gas

lift methods with maximum energy efficiencies of 30 [%] followed by intermittent gas lift which has the lowest efficiency in terms of energy from all available lifting methods. [4, pp. 5,6]

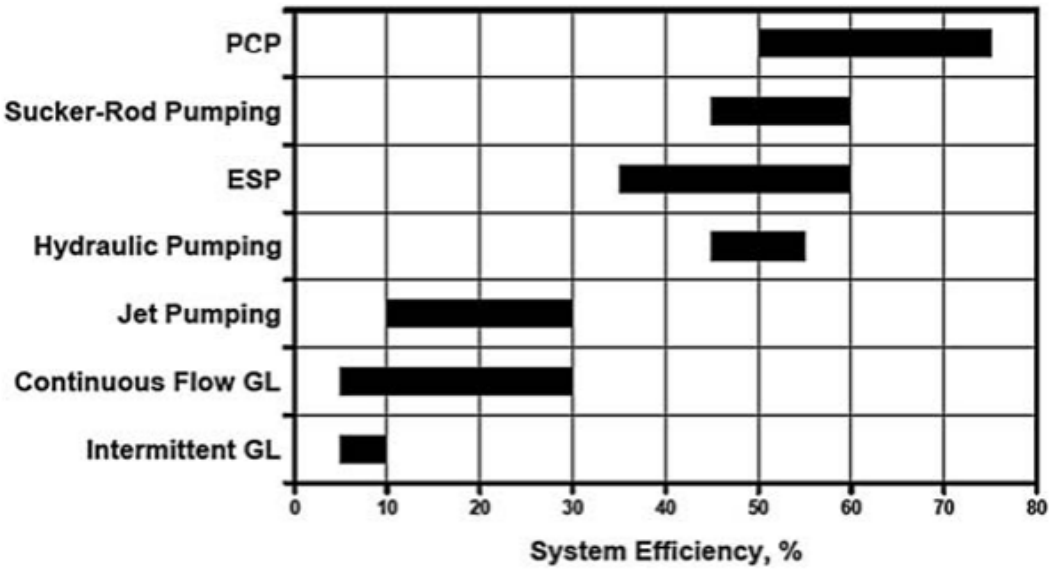

Figure 5: Energy Efficiencies of Artificial Lift Methods [4, pp. 5]

2.9 Electrical Submersible Pump

Pumps used in the oil and gas industry can be divided into two groups. One group are displacement pumps also known as positive displacement pumps with sucker rod pumps and progressive cavity pumps as examples. The second group is dynamic pumps where electrical submersible pumps belong to. An ESP is a centrifugal pump driven by an electric motor. The fluid is lifted through the pump due to an energy conversion from kinetic to pressure energy. Submersible pumps that are used in ESP installations operate with their shafts in vertical position. Normally these pumps are built as multistage pumps with tens to hundreds of stages in serial alignment and have a radial or mixed flow configuration. Moreover, the impellers are configurated in the closed vane design, the ESP does have a single suction side and they are self-priming. [4, pp. 23]

2.9.1 Centrifugal Pump operational Basics

The governing principle for the energy conversion in a centrifugal pump is described by the General Energy Equation stating that every change in energy of the fluid equals the work provided by the prime mover. In this energy conversion, the fluid undergoes three forms of energy starting with potential energy, transforming into kinetic energy, and finally converted to pressure energy. Since the summation of pressure and kinetic energy needs to be constant,

the energy provided by the prime mover is transformed into fluid pressure. The vertical elevation distance in each pump stage is neglected due to its marginal change in height.

The rotor, also known as an impeller, and the stator, also known as a diffusor, are the two primary components of a centrifugal pump. Figure 6 depicts a single-stage centrifugal pump configuration. The centrifugal pump's motion is provided by the impeller, which is made up of fully enclosed curved vanes. The primary mover produces torque, which is turned into kinetic energy. The diffusor on the other hand is a stationary part consisting of the motor casing, bearings, and seals. When liquid enters the vane channels of the diffusor, kinetic energy is transformed into pressure energy, allowing the liquid to be discharged at the top of the stage with a higher pressure level than that at the inlet of the impeller. Therefore, in a multistage centrifugal pump where the fluid leaves one stage at the discharge side and enters the following stage at the impeller, pressure is increased allowing the liquid to be pumped to the surface.

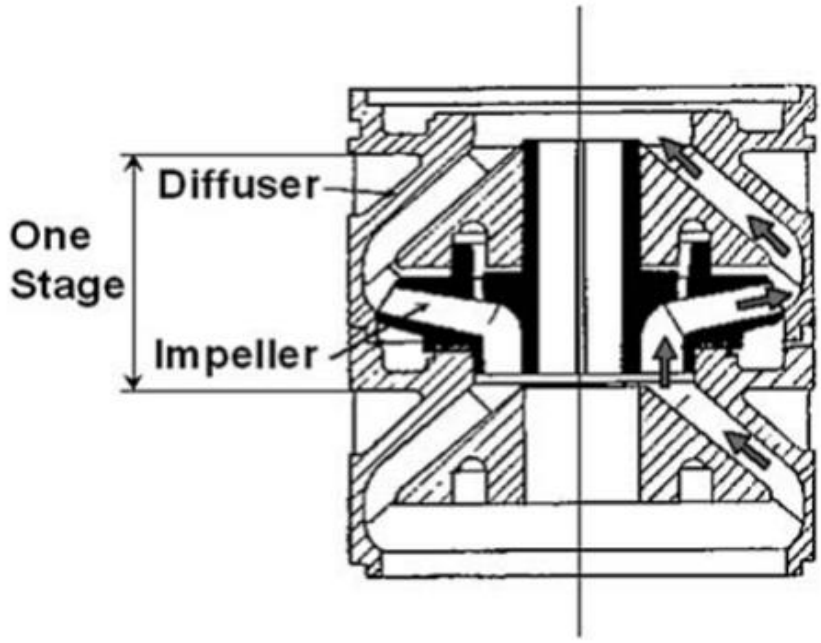

Figure 6: Single-Stage Mixed Flow Centrifugal Pump [4, pp. 24]

Centrifugal pumps are classified into three groups based on the orientation of the impeller discharge in radial, axial and mixed flow applications. While axial flow pumps are not utilized in ESP applications, the radial flow configuration is used for small capacity pumps with liquid rates up to 3000 [bpd], and the mixed flow design is applied for higher rates. Typically, impellers with backward curved vanes are used for ESP pumps, but also other designs such as radial or forward curved vanes are viable options. It is worth noting that as the liquid particles approach closer to the discharge, the cross-sectional area accessible for liquid flow between two subsequent vanes increases meaning that the energy conversion from kinetic to pressure

energy already starts at the impeller and is then completed by the diffusor for each subsequent pump stage.

Diffusers for radial flow pumps are part of the housing and the desired amount of pump stages is realized by stacking the appropriate number of impellers and diffusers on top of each other. The diffusor has a bore in the middle, therefore, the subsequent stage of the pump can be mounted on top by placing the impeller in the skirt bore and the impeller of the stage below is fitted inside the diffuser bore with its hub. The cross-sectional area between two successive vanes is the prerequisite for energy conversion. Due to an increase in this area, there is a conversion from kinetic energy to pressure energy. Radial flow impellers are mounted on the pump shaft with the hub and are rotated with keys that fit into the impeller's key-way. The impellers can either be free-floating allowing them to move up and down in an axial direction or they are axially fixed to the pump shaft and called fixed impellers. Additionally to the impeller vanes that are located between the top and bottom shroud, each impeller has two thrust washers, one on top and another one at the bottom usually made of laminated plastic to ensure low friction between the stationary diffuser and the rotating impeller.

The design of impellers and diffusers for mixed flow pumps differs in such that often certain balancing mechanisms are in place to reduce axial forces for each pump stage. This is conducted by balancing rings and balancing holes that connect the inlet of the impeller and discharge side which results in a reduced overall pump efficiency as a result of pressure decline per stage but effectively lowers axial forces acting on the impeller and diffuser. [4, pp. 23-27]

2.9.2 Pump Performance

A centrifugal pump transforms mechanical energy provided by the drive unit into kinetic energy of the transported fluid. Kinetic energy is proportional to the density multiplied by the square of the velocity. When the pump is operated at a given speed with a constant discharge velocity at the impeller, fluids with different densities get different amounts of energy. As a result, the energy conversion leads to a pressure increase in the pump with increasing density of the liquid transported. Normally when dealing with centrifugal pumps the pressure increase developed by the pump is divided by the liquid density resulting in the head. Since the head developed is constant for any given liquid, in contrast to pressure that depends on the liquid density, head is used in all calculations necessary to determine the centrifugal pump performance. To calculate the head developed by the impeller under optimal operating conditions where friction and additional losses are neglected is done with the Euler equation and the graphical result that shows head developed over the theoretical pumping rate is given in Figure 7.

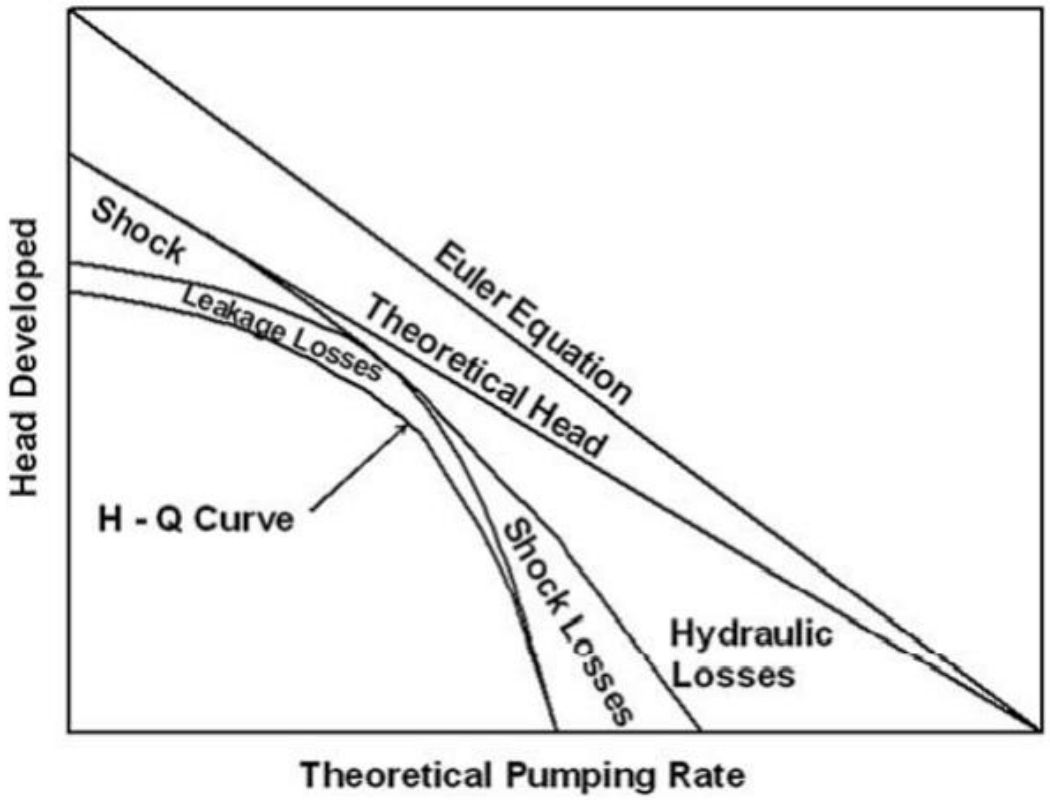

Figure 7: Derivation of a Pump's H-Q Curve [4, pp. 29]

The Euler equation however assumes an infinite number of vanes which is not applicable for real centrifugal pumps where the number of vanes is limited. Moreover, the liquid located between two successive vanes is exposed to centrifugal forces and develops a circulating type of flow which contributes to a change in velocity distribution and theoretical head developed.

In addition, several types of losses occur that alter the shape of the theoretical head resulting in the actual head developed by the pump. Shock losses occur due to sudden changes in flow direction at the inlet and outlet of the impeller, they are negligible at the best efficiency point but increase at lower and higher liquid rates. Fluid friction and diffusion losses in the impeller lead to hydraulic losses that steadily increase with liquid rate. Another problem is leakage losses. These occur due to the clearance between the rotating and fixed parts of the pump. Since the flow rate across the impeller is larger than the actual output of the stage, the produced head at any given liquid rate is reduced, however, leakage losses are reduced as the liquid rates increase. Considering all additional losses results in the H-Q curve that describes the actual pump behavior. The performance of real a centrifugal pump starts with the head developed per stage at the shut-off head where the flow rate equals zero and gradually decreases with increasing liquid rate independently of the liquid's density.

To pump the liquid to the surface and overcome all energy losses, the pump needs to be driven by the motor requiring a certain power that is represented by the brake horsepower (Figure 8). The useful hydraulic power can be derived from the pump curve. This power is valid for any given liquid rate and proportional to the product of the head, liquid capacity, and liquid density. While turbulent losses decrease towards the best efficiency point but are considerably high at low and high pumping rates, frictional losses in the channels of the impeller as well as leakage losses increase proportionally with increasing liquid rate. Disk friction losses are a result of the energy required to rotate the impeller in the liquid and are almost independent of the liquid rate, which also accounts for bearing losses that are due to mechanical friction losses in the stuffing box and bearings of the pump.

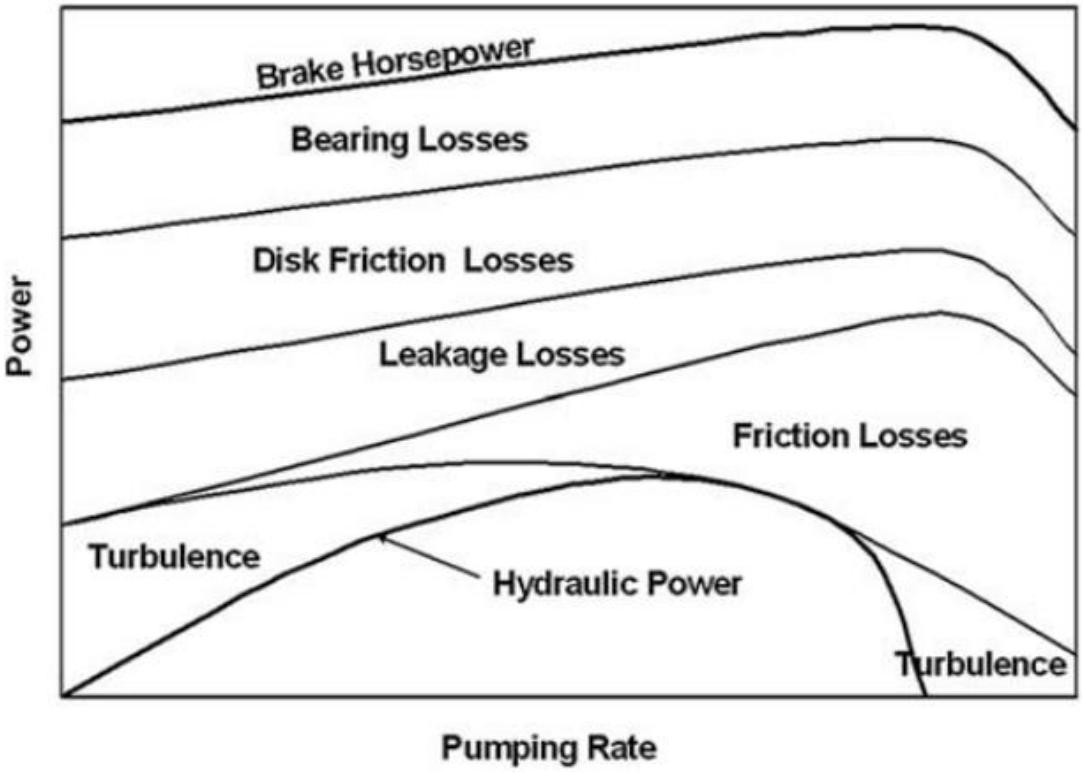

Figure 8: Power Conditions in a Centrifugal Pump Stage [4, pp. 30]

Testing of centrifugal pumps is conducted at a constant speed with varying pumping rates adjusted by throttling the flow at the pump discharge. API RP 11S2 recommends running the tests with freshwater and a temperature of 60 [°F]. The rotational speed is set to 3,500 [rpm] for 60 [Hz] or 2,917 [rpm] for 50 [Hz]. If tests are conducted with fluids other than freshwater, the pump manufacturer has to correct the test results to the recommended standard conditions. This also applies if tests are run with multistage pumps as the performance curves must represent the pump operation for one stage. Such pump tests deliver important information about certain parameters such as liquid flow rate, pressures at the pump suction and pump discharge, as well as break horsepower. The pump efficiency curve is a result of dividing the

useful hydraulic power required to transfer the fluid by the break horsepower needed to drive the pump. By plotting the pump efficiency curve as a function of the flow rate (Figure 9) it can be seen that it follows the same shape as the hydraulic power with a decline at both, low and high flow rates. The pump efficiency indicates how well the pump can convert the mechanical energy input from the driving unit into hydraulic power required to pump fluids. The pump manufacturer should additionally provide pump performance curves. These include the head curve, the brake horsepower, and the pump efficiency. Both, the head created by the pump and the break horsepower which is required to drive the pump are given as functions of the flow rate.

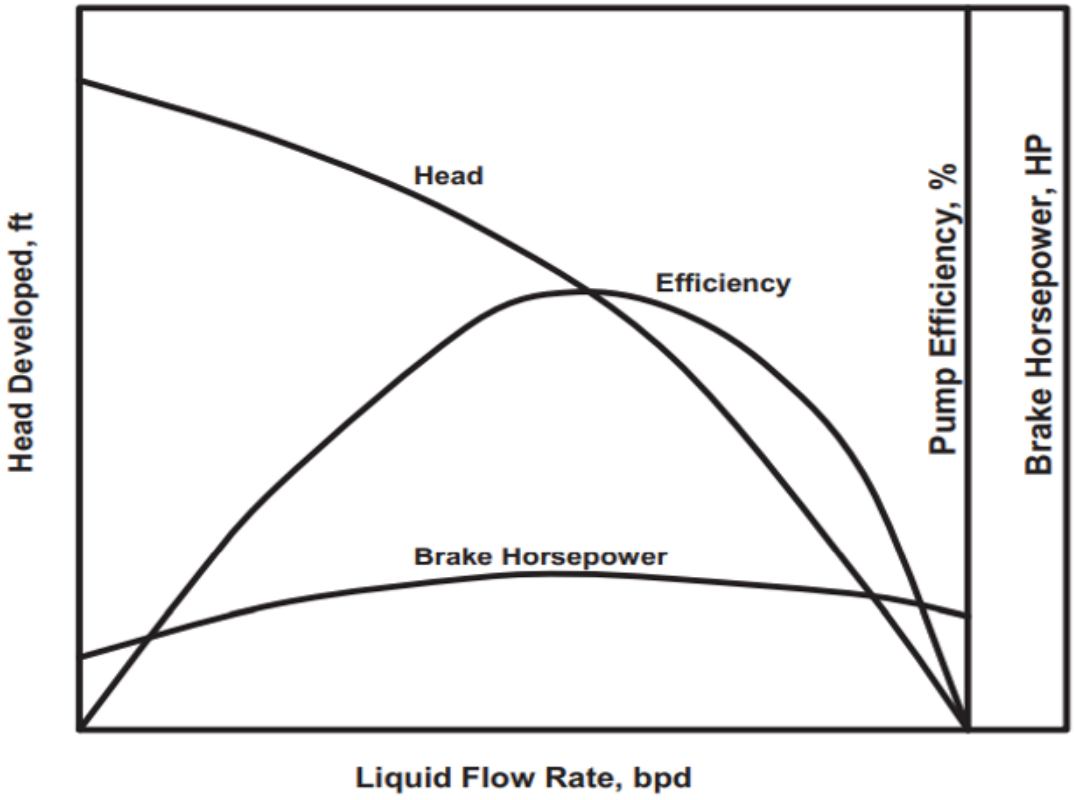

Figure 9: Schematic Pump Performance Curves [4, pp. 31]

Fluctuations in pump manufacturing lead to variances in performance and therefore to a deviation from the published performance curves. The pump manufacturer needs to accomplish accepted tolerances between the actual performance curves of the pump and the published curves. The best efficiency point of the pump at a nominal flow rate needs to be at least 90 [%] of the published value. Moreover, the pump flow rate curve should be in the range of +-8 [%] of the recommended range, and the head flow rate tolerance should be within +-5 [%] of the recommended performance curve operating range. [4, pp. 28-31, 59-61]

2.9.3 Axial Thrust Forces

Axial and radial forces act on the pump impeller during operation and are communicated to the pump shaft. Because these forces are handled by the ESP housing, radial force components do not affect the current operation. Axial forces, on the other hand, must be taken into account by properly designed thrust bearings, as they can harm the pump's condition by causing axial movement of the impellers and shaft, particularly when the pump is designed for submersible operation with tens to hundreds of stages. Axial forces belong to two designated groups being either static or dynamic. While the weight of the pump and impeller contribute to static forces and act downwards, dynamic forces are due to liquid pumped through the consecutive stages and can either act down- or upward. Forces acting on the impeller shroud as well as forces acting on the cross-sectional area of the pump point downward. They result from suction and discharge pressures and axial loads originating from the pump discharge pressure, respectively. Inertial forces on the other hand act upward as a result of changing flow direction inside the pump stage. The pump manufacturer must designate an operating region in terms of flow rate for each pump. This ensures a safe operation since axial thrust changes with flowrate as depicted in Figure 10. At the shut-off condition which equals zero flow rate thrust is at a maximum and continuously decreases with increasing liquid rate until it reaches the balanced condition whereafter, thrust changes the direction and the upthrust region starts.

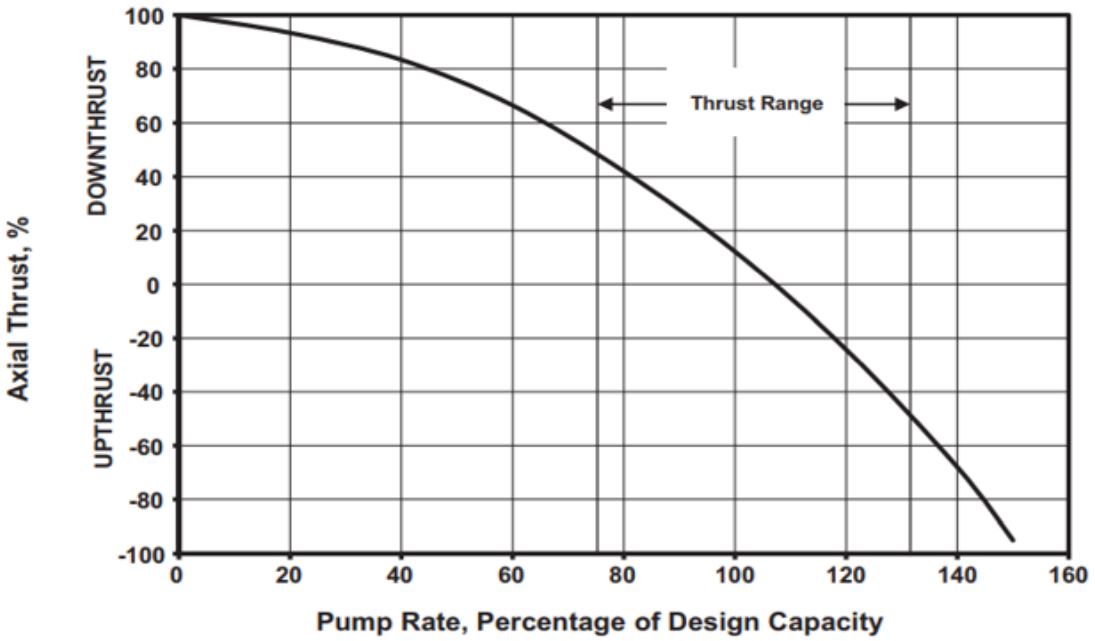

Figure 10: Variation of Axial Thrust with Flow Rate [4, pp. 35]

The elimination of axial forces can be accomplished with two different impeller designs.

One option is to use fixed impellers where all occurring axial forces are directly transmitted to the pump shaft. In this configuration, the impellers are locked to the pump shaft in the axial

direction without distance between subsequent hubs enabling a pump operation outside of the recommended operating window with relatively low damage to the stages. These so-called compression pumps are utilized in ESP applications capable of producing higher liquid rates and are also able to tolerate fluids with abrasives. This solution requires relatively large thrust bearings since all axial forces are taken by the main thrust bearing located in the ESP units protector section. Additional aspects in terms of limitations are higher investment costs due to manufacturing requirements for precise fitting of impellers along the pump shaft and a maximum number of 80-100 stages.

The other option is to install floating impellers where most of the axial forces act on the up-and downthrust washers located on the impellers. A part of the axial forces, however, is redirected towards the main thrust bearing located in the protector as the axial load reduces the gap between individual impellers resulting in a downward thrust acting on the pump shaft. The special design of floating impellers allows building pumps with up to several hundred stages while installing smaller-capacity thrust bearings in the protector as most of the thrust occurring during operation is absorbed inside the pump. Furthermore, these pumps have lower investment costs compared to their counterpart with fixed impellers and also relinquish axially fixing the impellers on the shaft which is time-consuming work requiring high precision. In terms of limitations, the most important factor is given by the annular space available in the casing since the load capacity of the thrust bearings depends on their size. As a result, pumps are manufactured in smaller sizes with diameters up to 6 [in] and smaller operating ranges compared to pumps with fixed impellers. [4, pp. 32-35, 61-67]

2.10 Electrical Submersible Pump Motor

The most commonly used drive units for electrical submersible pumps are three-phase, two-pole, squirrel cage AC induction motors. They are very popular in oil field applications due to their simple construction and their high efficiency compared to other conventional motor types. The governing principle for these motors is electromagnetic induction which leads to electric current induced as a conductor moves in a magnetic field.

The standing part of the motor, the so-called stator, generates the magnetic field and contains one coil for each phase. As the magnetic poles of the electromagnet change their direction twice for each cycle, the magnetic field rotates accordingly to the change in direction of the AC. The stator is a hollow cylinder composed of tightly packed thin magnetic steel discs and press-fit into the housing. These so-called laminations are thin steel discs that are insulated with a coating on both sides. As these steel discs are pressed together, they build the core of the stator windings and by realizing such a solution, the occurrence of wasteful eddy currents is prevented

which is otherwise inevitable in stators composed of solid steel. Inside the stator slots are copper stator windings that are connected to the AC power. It is important to insulate these wires to ensure protection against wire-to-wire contact. Three pairs of coils are displaced at 120 degrees along the perimeter of the motor. Furthermore, each pair's coils are facing each other on the opposite side of the stator. The three coils are then linked to the three phases in “Y” connection (Figure 11). The so-called end turn provides phase-to-phase insulation by redirecting the coils in a 180-degree turn at the two ends of the lamination stack. In general, insulation is very important to prevent any electrical failures that might occur. Therefore, a sophisticated insulation system needs to be in place. The individual wires that form up the windings are insulated as well as the space between the stator and the windings. Furthermore, protection against phase-to-phase faults needs to be implemented and the stator is insulated in addition to the previously implemented measures. Finally, all the void space in the slots and end turns is filled with epoxy and results in increased mechanical strength, prevention of wire movement, and improved dielectric strength of the windings. Due to its greater heat capacity that is about 300 times higher than that of varnish which is an outdated version compared to the solution that utilizes epoxy, heat dissipation to the outside of the motor due to heat generation in the stator windings is greatly enhanced.

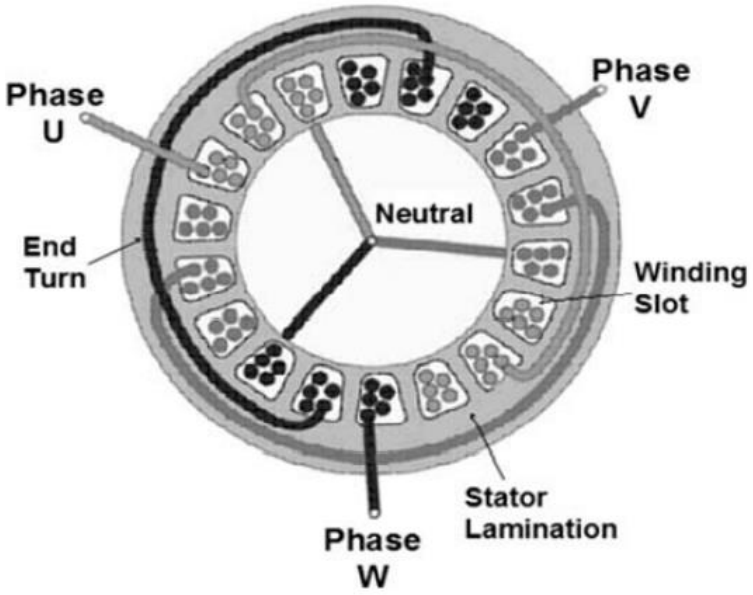

Figure 11: Y-Connected Windings in the Stator [4, pp. 74]

The squirrel-cage type rotor which is isolated from the stator by a narrow air gap is located inside the stator and is attached to the shaft. Since the rotor and the power source are not connected with each other, this type of rotor counts as one of the most reliable. The stator windings lead to a rotating magnetic field that induces an AC flow in the motor which transforms the rotor into a set of electromagnets. The rotor itself consists of copper bars that

are short-circuited by two copper end rings. These copper bars are inserted in slots provided by the magnetic rotor laminations to prevent eddy currents similarily to the principle used in the stator. Continuous rotation of the motor is achieved due to attraction and repulsion between the unlike and like poles of the stator and the poles of the magnetic field from the motor.

The term asynchronous motor originates from the slower speed at which the rotor revolves compared to the synchronous speed of the motor. This speed difference, commonly known as motor slip, results from electromagnetic induction and leads to a relative movement between the magnetic field from the stator and the wires of the rotor.

Application in the oil and gas industry requires certain design changes and considerations due to the limitations and requirements present. One limiting factor is given by the casing size which results in a greater length-to-diameter ratio compared to that of surface motors. Therefore, an increase in motor power can only be realized by increasing the length of the unit since the radial space is limited. Another factor is motor cooling. Usually, surface motors are cooled by the surrounding air. The same principle is not applicable to motors inside wells. The only possibility to cool the motor is due to the convective heat transfer from the well fluid that flows past the motor. This however brings benefits since the liquid has a much higher head capacity when compared to air. The resulting higher cooling effect allows for currents that are ten times higher than those available for surface motors without running into the danger of overheating. Another benefit is that ESP motors have exceptional low inertia allowing them to accelerate to full speed in less than 0.2 seconds right from the start. Due to limited space inside the well, the power supply is provided from the surface by long well cables which results in substantial voltage drops. [4, pp. 72-75]

Chapter 3

Mathematical Model

3.1 Electrical Drive Unit

There are several types of models available like space vector phase theory or two-axis theory of electrical machines. Because energy transmission is represented by steady-state values, it is useful to describe electric machines as though they are direct current machines from the perspective of control systems. On the electrical side, voltages and currents remain constant, so they do not fluctuate over time, making control optimization easier. To model an AC machine as a DC machine the Clarke Park transform or dq transform can be utilized. [6, pp. 2,3]

3.1.1 Park Transformation

Clark's transformation converts currents and voltages in a stationary reference frame as space vectors, meaning that the stationary three-phase quantities a, b, and c are transformed to α and β. Park's transformation then converts these stationary quantities to an equivalent rotating reference frame, hence from α and β to d and q. [7, pp. 89-96]

The Park transformation that implements the transform for an abc -phase to $dq0$ -phase alignment used in the Matlab Simulink model is shown in Equation (1)

$$\begin{pmatrix} V_{ds} \\ V_{qs} \\ V_0 \end{pmatrix} = \frac{2}{3} \begin{pmatrix} \sin(\theta) & \sin(\theta - \frac{2\pi}{3}) & \sin(\theta + \frac{2\pi}{3}) \\ \cos(\theta) & \cos(\theta - \frac{2\pi}{3}) & \cos(\theta + \frac{2\pi}{3}) \\ \frac{1}{2} & \frac{1}{2} & \frac{1}{2} \end{pmatrix} \begin{pmatrix} V_a \\ V_b \\ V_c \end{pmatrix} \quad (1)$$

where:

$V_a, V_b,$ and V_c are the supply voltages of the three-phase system in the abc reference frame

V_{ds} and V_{qs} are the voltage components of the two-axis system in the rotating reference frame

V_0 is the zero voltage component of the two-axis system in the stationary reference frame

θ is the angle between the a and q axis alignment, hence the position of the rotor.

[8]

The position of the rotor θ equals the integral of the angular velocity of the motor ω_r and is given by Equation (2)

$$\theta = \int \omega_r \, dt \tag{2}$$

The equivalent circuits of the induction machine for the quadrature axis and direct axis are shown in Figure 12 and Figure 13 respectively.

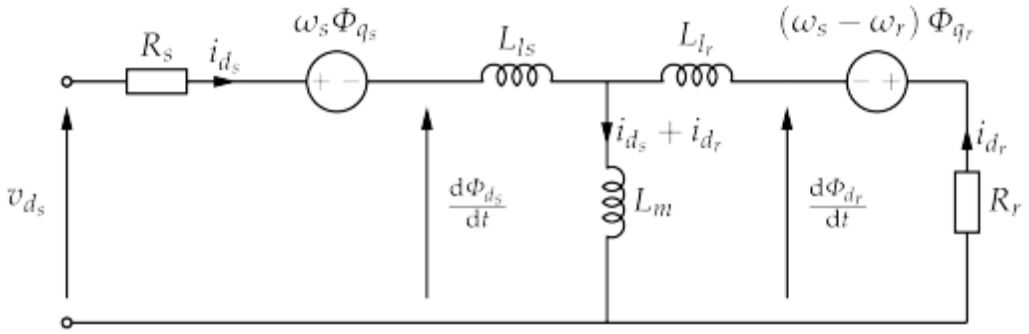

Figure 12: 3-Phase, Symmetrical Induction Machine Reference Frame Equivalent in q-Variables [6, pp. 3]

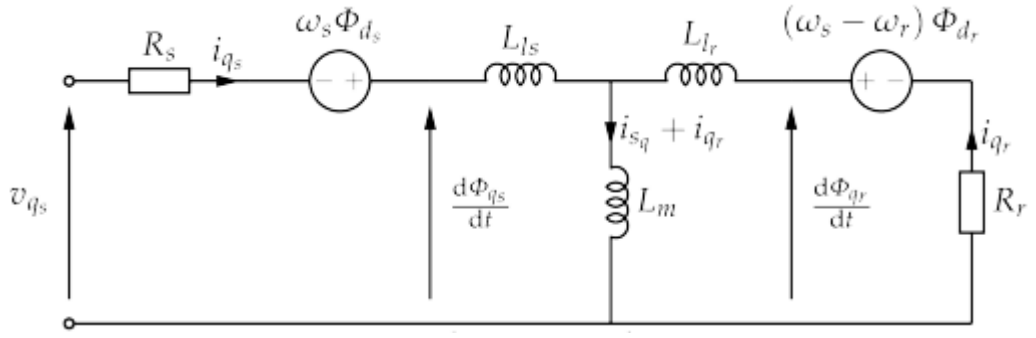

Figure 13: 3-Phase, Symmetrical Induction Machine Reference Frame Equivalent in d-Variables [6, pp. 3]

The stator winding series resistance Rs represents the finite direct current resistance of the stator winding and the rotor series resistance Rr represents the finite direct current resistance of the rotor windings or bars. The stator winding leakage inductance Lls represents the magnetic flux around the stator windings caused by the current passing through the stator windings. This inductance reflects the fraction of the stator flux that does not couple the stator to the rotor,

hence, it does not have the chance to generate a current in the rotor because rotor bars/ windings are not cut. The rotor winding leakage inductance Llr represents the magnetic flux around the rotor bars or windings caused by the current induced to the rotor from the stator magnetic field. Lm is the mutual inductance that couples the rotor and the stator.

The back electromotive force of a stator on the d axis is proportional to the synchronous speed and flux on the q axis. The current produces a magnetic flux, and the rate of change of that magnetic flux generates a voltage across the winding through which the current travels. The back electromotive force will act to oppose the change of the current. The direct axis and quadrature axis are perpendicular to each other. Therefore the electromotive force felt on the direct axis is due to the flux on the quadrature axis. Similarly, the electromotive force felt on the quadrature axis is caused by the direct axis flux. The back electromotive force of the rotor on the d axis is proportional to the difference between the synchronous speed and the rotor speed as well as the rotor flux that is generated by the q axis.

The rate of change of flux for the stator on the d axis is

$$\frac{d\Phi_{ds}}{dt} = v_{ds} - i_{ds} R_s - \omega_s \Phi_{qs} \tag{3}$$

and for the stator on the q axis is

$$\frac{d\Phi_{qs}}{dt} = v_{qs} - i_{qs} R_s + \omega_s \Phi_{ds} \tag{4}$$

Similarly, the rate of change of flux for the rotor on the d axis is

$$\frac{d\Phi_{dr}}{dt} = - i_{dr} R_r - (\omega_s - P * \omega_r) \Phi_{qr} \tag{5}$$

and for the rotor on the q axis is

$$\frac{d\Phi_{qr}}{dt} = - i_{qr} R_r + (\omega_s - P * \omega_r) \Phi_{dr} \tag{6}$$

The rotor and stator flux on the d and q axis are linked by the following expressions starting with the q axis stator flux

$$\Phi_{qs} = (i_{qs} + i_{qr}) L_m + i_{qs} L_{ls} \tag{7}$$

The d axis stator flux is

$$\Phi_{ds} = (i_{ds} + i_{dr}) L_m + i_{ds} L_{ls} \tag{8}$$

and the q axis rotor flux and d axis rotor flux are

$$\Phi_{qr} = \left(i_{qs} + \ i_{qr}\right)L_m + \ i_{qr}\, L_{lr} \tag{9}$$

$$\Phi_{dr} = (i_{ds} + \ i_{dr})L_m + \ i_{dr}\, L_{lr} \tag{10}$$

respectively.

A three-phase induction machine in the Park frame may be simulated using either flux or currents as a state variable. The technique in which the current is impressed and the resulting electromagnetic field on the stator is computed together with all mechanical outputs necessitates the use of derivatives in the calculations. However, if this machine model is fitted with power electronics, it will accept the anticipated currents independent of other influences in the system, which might increase noise and lead to instabilities such as lack of convergence. Using the machine model with flux as state variable results in less complicated equations. It is required to express the flux equations in terms of the d and q axis since the simulation will be run with a voltage applied to the stator winding. Computing the rate of change of the flux with the voltage and integrating yields the flux. The currents are then calculated using the flux and sent back into a regulated current source that is situated between the terminals in which the voltage was impressed.

Rearranging the flux Equations (7)-(10) in terms of currents leads to the q axis stator current

$$i_{qs} = \frac{\Phi_{qs} - \ L_m\, i_{qr}}{L_m\, L_{ls}} \tag{11}$$

And the d axis stator current

$$i_{ds} = \frac{\Phi_{ds} - \ L_m\, i_{dr}}{L_m\, L_{ls}} \tag{12}$$

As well as the q axis rotor current

$$i_{qs} = \frac{\Phi_{qs} - \ L_m\, i_{qr}}{L_m\, L_{lr}} \tag{13}$$

and the d axis rotor current

$$i_{qs} = \frac{\Phi_{qs} - \ L_m\, i_{qr}}{L_m\, L_{lr}} \tag{14}$$

The solutions of the current equations, as well as the flux equations, are interdependent meaning that the build-in solver of Matlab Simulink must solve them simultaneously.

where:

v_{ds} and v_{qs} are the d-axis and q-axis voltages of the stator [V]

ω_s and ω_r are the stator and rotor angular velocities [rad s^{-1}]

R_s and R_r are the stator and rotor winding series resistances [Ohm]

L_m is the mutual inductance coupling stator and rotor [mH]

L_{ls} and L_{lr} are the stator and rotor winding leakage inductances [mH]

P is the number of pole pairs [-]

[6]

3.1.2 Electromagnetic Torque

The electromagnetic torque T_e results from the interaction of the axial currents in the rotor bars and the radial flux wave and is calculated according to Equation (15). The electromagnetic torque acts in the same direction as the rotating field and the rotor is dragged along by the field. Due to the slip, the rotor can't catch up with the field as this would result in no rotor electromagnetic field, no currents induced, and therefore, no torque produced.

$$T_e = P(i_{qs}\big((i_{ds}\, i_{dr})L_m\big) + i_{ds}\left(\big(i_{qs} + i_{qr}\big)L_m\right) \tag{15}$$

[6, pp. 7]

3.1.3 Rotor Speed

The rate of change of speed of the induction motor is given by Equation (16)

$$\frac{d\omega_r}{dt} = \frac{(T_e - T_L - D\omega_r)}{J} \tag{16}$$

where:

ω_r is the angular velocity of the rotor [rad s^{-1}]

D is the drag coefficient due to friction [Nm/(rad s^{-1})]

T_L is the load torque [Nm]

J is the sum of mechanical inertia of the rotating parts [kg m^2]

[6, pp. 7]

3.2 Pump Performance Curves

The pump head curve model used to represent the centrifugal pump is a polynomial function (Equation(17)) [9, pp. 3]. It gives a relationship between the produced pump head H [m] and the flow rate q [m^3/s] and angular velocity ω [rad/s].

$$H_n = a\,\omega^2 + b\,q_n\,\omega + c\,{q_n}^2 \tag{17}$$

The equation contains three parameters a, b, and c that need to be identified for the given system. These parameters are identified with the simplest version of linear least-squares methods, the method of ordinary least squares, and the resulting matrix equation is then solved in Matlab.

Given are the data $\{(H_1, q_1), \dots, (H_N, q_N)\}$, and the associated error E for $H_n = a\,\omega^2 + b\,q_n\,\omega + c\,{q_n}^2$ is defined by

$$E(a,b,c) = \sum_{n=1}^{N} [H_n - (\mathrm{a}\,\omega^2 + b\,\omega\,q_n + c\,{q_n}^2)\,]. \tag{18}$$

This equation states that the error E is n times the variance of the given data set $\{H_1 - (\mathrm{a}\,\omega^2 + b\,\omega\,q_1 + c\,{q_1}^2)\,, \dots, H_N - (\mathrm{a}\,\omega^2 + b\,\omega\,q_N + c\,{q_N}^2)\,\}$, and a function of the three variables a, b, and c. According to multivariable calculus, the necessary condition for the error E to be a minimum is

$$\frac{\partial E}{\partial a} = 0, \qquad \frac{\partial E}{\partial b} = 0, \qquad \frac{\partial E}{\partial c} = 0. \tag{19}$$

Differentiating $E(a,b,c)$ results in

$$\frac{\partial E}{\partial a} = \sum_{n=1}^{N} 2\,[H_n - (a\,\omega^2 + b\,q_n\,\omega + c\,{q_n}^2)] \cdot (-\omega^2) \tag{20}$$

$$\frac{\partial E}{\partial b} = \sum_{n=1}^{N} 2\,[H_n - (a\,\omega^2 + b\,q_n\,\omega + c\,{q_n}^2)] \cdot (-\omega\,q_n) \tag{21}$$

$$\frac{\partial E}{\partial c} = \sum_{n=1}^{N} 2\,[H_n - (a\,\omega^2 + b\,q_n\,\omega + c\,{q_n}^2)] \cdot (-{q_n}^2) \tag{22}$$

When $\partial E/\partial a = \partial E/\partial b = \partial E/\partial c = 0$, the normal equations of the given problem are

$$\sum_{n=1}^{N} [H_n - (a\,\omega^2 + b\,q_n\,\omega + c\,{q_n}^2)] \cdot \omega^2 = 0 \tag{23}$$

$$\sum_{n=1}^{N}[H_N - (a\,\omega^2 + b\,q_n\,\omega + c\,{q_n}^2)]\cdot\omega\,q_n = 0 \tag{24}$$

$$\sum_{n=1}^{N}[H_N - (a\,\omega^2 + b\,q_n\,\omega + c\,{q_n}^2)]\cdot{q_n}^2 = 0 \tag{25}$$

These normal equations expressed as a matrix equation yields

$$\begin{pmatrix} \sum_{n=1}^{N}\omega^4 & \sum_{n=1}^{N}\omega^3\,q_n & \sum_{n=1}^{N}\omega^2\,{q_n}^2 \\ \sum_{n=1}^{N}\omega^3\,q_n & \sum_{n=1}^{N}\omega^2\,{q_n}^2 & \sum_{n=1}^{N}\omega\,{q_n}^3 \\ \sum_{n=1}^{N}\omega^2\,{q_n}^2 & \sum_{n=1}^{N}\omega\,{q_n}^3 & \sum_{n=1}^{N}{q_n}^4 \end{pmatrix}\begin{pmatrix} a \\ b \\ c \end{pmatrix} = \begin{pmatrix} \sum_{n=1}^{N}\omega^2\,H_n \\ \sum_{n=1}^{N}\omega\,H_n\,q_n \\ \sum_{n=1}^{N}H_n\,{q_n}^2 \end{pmatrix} \tag{26}$$

This matrix equation with the form $A\,x = B$ is rearranged to the form of $x = A^{-1}\,B$ and results in

$$\begin{pmatrix} a \\ b \\ c \end{pmatrix} = \begin{pmatrix} \sum_{n=1}^{N}\omega^4 & \sum_{n=1}^{N}\omega^3\,q_n & \sum_{n=1}^{N}\omega^2\,{q_n}^2 \\ \sum_{n=1}^{N}\omega^3\,q_n & \sum_{n=1}^{N}\omega^2\,{q_n}^2 & \sum_{n=1}^{N}\omega\,{q_n}^3 \\ \sum_{n=1}^{N}\omega^2\,{q_n}^2 & \sum_{n=1}^{N}\omega\,{q_n}^3 & \sum_{n=1}^{N}{q_n}^4 \end{pmatrix}^{-1}\begin{pmatrix} \sum_{n=1}^{N}\omega^2\,H_n \\ \sum_{n=1}^{N}\omega\,H_n\,q_n \\ \sum_{n=1}^{N}H_n\,{q_n}^2 \end{pmatrix} \tag{27}$$

[10, pp. 4,5]

The matrix equation is solved in a Matlab program as follows:

```
clear all; close all; clc

%H=[234;234.13;231.39;225.79;217.31;205.96;191.75;174.66;154.70;131.88];
%Q=[0;0.002;0.004;0.006;0.008;0.010;0.012;0.014;0.016;0.018];

% Input parameters for head H and flowrate Q from pump manufacturer
% (Schlumberger REDA ESP D2400 50Hz/2917 rpm)
H=[7.5;7.49;7;6.8;5.9;5.5];
Q=[0;0.0005787;0.0011574;0.001736;0.0028935;0.0034722];

H1=sum(H);
Q1=sum(Q);

%w=300;
%n=10;
w=305;
n=6;

Q4=Q.^4;
Q3=Q.^3;
Q2=Q.^2;
Q1=Q.^1;
```

```
sumQ4=sum(Q4);
sumQ3=sum(Q3);
sumQ2=sum(Q2);
sumQ1=sum(Q1);

D=sum(w^2*H);
E=sum(w*H.*Q);
F=sum(H.*Q.^2);

A=[w^4*n  w^3*sumQ1  w^2*sumQ2;w^3*sumQ1  w^2*sumQ2  w*sumQ3;w^2*sumQ2  w*sumQ3
sumQ4];
B=[D;E;F];

p=inv(A)*B;
disp(p(1));
disp(p(2));
disp(p(3));

scatter(Q,H)
hold on
plot(Q,p(1)*w^2+p(2)*Q*w+p(3)*Q.^2)
```

The solution of the Matlab program for the parameters a, b, and c results in:

$$\begin{cases} a = 8.1296e-5 \\ b = -1.0234 \\ c = -8.4131e4 \end{cases}$$

Thus, the head developed by the pump expressed as polynomial function is:

$$H = 8.1296e-5\ \omega^2 - 1.0234\ q\ \omega - 8.4131e4\ q^2 \tag{28}$$

and is graphically presented in Figure 14.

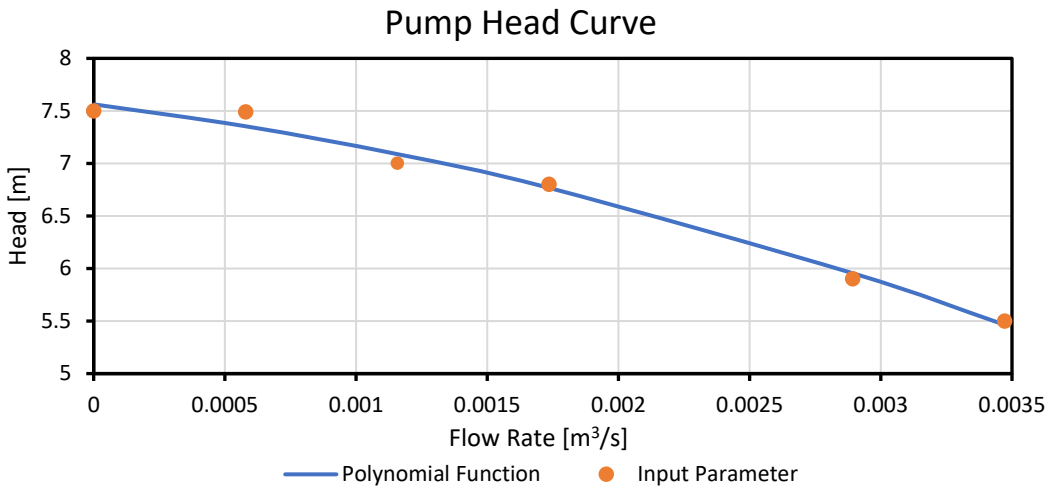

Figure 14: Pump Head over Flow Rate Polynomial Match

Similarly to the pump head curve polynomial function, also the pump torque is described with a polynomial function (Equation (29)) [9, pp. 3] where the torque T_P [Nm] is related to the flowrate q [m^3/s] and the angular velocity ω [rad/s].

$$T_P = a_t\, q^2 + b_t\, q\, \omega + c_t\, \omega^2 \tag{29}$$

The identification of the parameters a_t, b_t and c_t is conducted by utilizing the physical relationship that the pump power P_P [W] is a function of the angular velocity ω [rad/s] and the pump torque T_P [Nm], shown in Equation (30).

$$P_P = \omega\, T_P \tag{30}$$

The torque is calculated by graphically estimating values for the pump power P_P from the break horsepower curve from three distinct points shown in Figure 15.

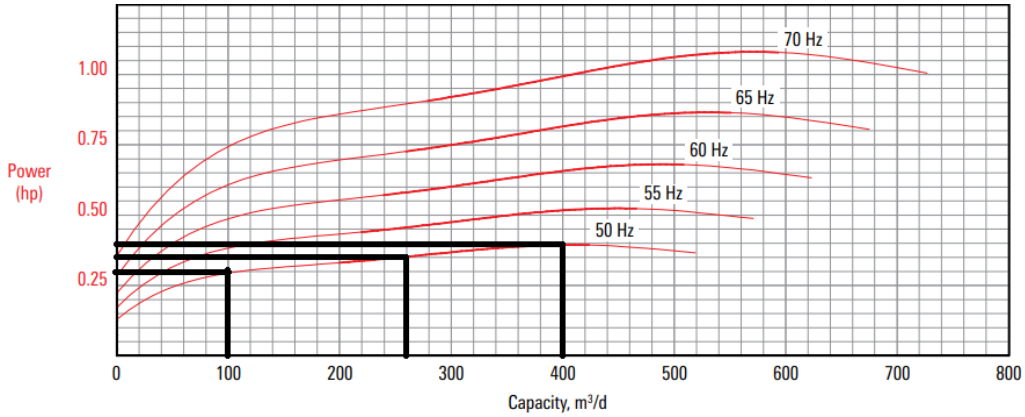

Figure 15: Pump Power over Flow Rate [11, pp. 86]

This results in a system of three equations containing the parameters a_t, b_t and c_t , and the solution of this system gives:

$$\begin{cases} a_t = -5.8041e6 \\ b_t = 142.6683 \\ c_t = 5.2585e-4 \end{cases}$$

Thus, the pump torque polynomial function is

$$T_P = -5.8041e6\, q^2 + 142.6683\, q\, \omega + 5.2585e-4\, \omega^2 \tag{31}$$

[12, pp. 30, 31]

and is graphically presented in Figure 16.

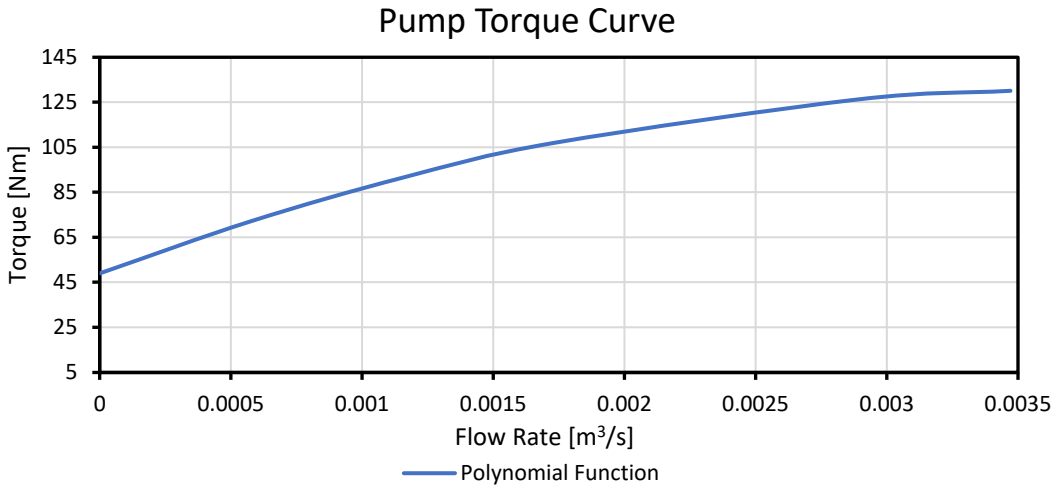

Figure 16: Pump Torque over Flow Rate Polynomial Function

3.3 Hydraulic Subsystem

The hydraulic subsystem includes the centrifugal pump model, pipes that connect the water tank with the pump as well as valves to further adjust the flow rate of the whole system.

3.3.1 Pump Flow Rate

The flow rate of a centrifugal pump depends on the pump head produced by the centrifugal pump and the system head produced from all other installations in the hydraulic subsystem. According to Newton's second law under the consideration of incompressible fluids flowing through a segment of a pipe with a constant cross-sectional area a mass element is exposed to two forces due to the pressure acting on each side, it can be stated that

$$m\dot{v} = F_1 - F_2 \tag{32}$$

where:

m is the mass of the fluid element inside the pipe

$\dot{v}$ is the rate of change of velocity

F_1 and F_2 are the acting forces

Since both forces F_1 and F_2 are a result of pressure, the formula $F = pA$ can be applied to Equation (32) leading to

$$m\dot{v} = A(p_1 - p_2) = A\Delta p \tag{33}$$

where:

A is the cross-sectional area of the pipe segment

p_1 and p_2 are the pressures acting on the left and right side of the fluid segment respectively

Δp is the pressure difference of p_1 and p_2

The volume of the fluid element is given by $V = LA$ and the mass of the fluid element is given by $m = \rho V$, with ρ being the fluid density and V being the volume of the pipe element, Equation (33) can be rewritten as

$$\rho LA\dot{v} = A\Delta p \tag{34}$$

The mass flow is calculated according to $q = \rho vA$, therefore the rate of change of mass flow can be calculated as $\dot{q} = \rho \dot{v} A$ and by inserting into equation (34) yields

$$\dot{q}L = A\Delta p \tag{35}$$

[13, pp. 16, 17]

Expressing Equation (35) in terms of the fluid head leads to

$$\frac{dq}{dt} = \frac{gA}{l_{pipe}} \Delta H \tag{36}$$

where:

ΔH is the head difference [m]

l_{pipe} is the length of the pipe system [m]

Substituting the head difference ΔH with the produced pump head, by inserting the polynomial pump head function, and the system head H_{sys} , leads to the final expression of the pump flow rate shown in Equation (37)

$$\frac{dq}{dt} = \frac{gA}{l_{pipe}} (a_p \omega_r^2 + b_p \omega_r q + c_p q^2 - H_{sys}) \tag{37}$$

[12, pp. 28]

3.3.2 Static Head

The static head loss is due to the height difference from the water tank outlet to the centrifugal pump inlet and is calculated after Equation (38).

$$H_S = h_2 - h_1 \tag{38}$$

where:

h_2 is the centrifugal pump inlet from reference height [m]

h_1 is the water tank outlet from reference height [m]

[12, pp. 29]

3.3.3 Velocity Head

According to Equation (39), the velocity head represents hydraulic losses due to the liquid flowing inside the pipe under the assumption that the velocity inside the tank equals zero

$$H_V = \left(\frac{4 * q}{\pi * D_{pipe}^2}\right)^2 * \frac{1}{2 * g} \tag{39}$$

where:

q is the flow rate of the centrifugal pump [m^3s^{-1}]

D_{pipe} is the pipe inside diameter [m]

[12, pp. 29]

3.3.4 Local Head

The local head includes losses due to changes in pipe geometry, sudden contractions along the pipe as well as both valves installed in the hydraulic system and is calculated according to Equation (40).

$$H_{Llocal} = \frac{1}{g} * \left(K_{mp} + K_{pt} + K_{v1} + K_{v2}\right) * \left(\frac{4 * q}{\pi * D_{pipe}^2}\right)^2 \tag{40}$$

where:

K_{mp} is the local loss coefficient due to sudden pipe contraction [-]

K_{pt} is the local loss coefficient due to changes in pipe geometry [-]

K_{v1} and K_{v2} are the local loss coefficients from valve 1 and valve 2 respectively [-]

[12, pp. 29]

Valve Model

$$K_{v1} = \frac{K + (0.5 * (1 - \beta_{v1}^2) + (1 - \beta_{v1}^2))^2}{\beta_{v1}^4} \tag{41}$$

$$K_{v2} = \frac{K + (0.5 * (1 - \beta_{v2}^2) + (1 - \beta_{v2}^2))^2}{\beta_{v2}^4} \tag{42}$$

$$\beta_{v1} = \frac{d_1}{D_{pipe}} \tag{43}$$

$$\beta_{v2} = \frac{d_2}{D_{pipe}} \tag{44}$$

[14]

3.3.5 Reynolds Number

The Reynolds number (Equation (45)) is a dimensionless parameter used to classify the flow and depends on the pipe diameter, flow rate, liquid viscosity, and liquid density. With Reynolds numbers smaller than 2000 to 2100, flow falls into the laminar regime, whereas Reynolds numbers larger than 4000 indicate turbulent flow.

$$Re = \frac{\rho_w}{\mu_w} * D_{pipe} * v \tag{45}$$

where:

ρ_w is the fluid density [kg/m^3]

μ_w is the fluid dynamic viscosity [Pa s]

$v = \frac{q}{A}$ is the fluid velocity [m/s]

[15, pp. 9-11]

3.3.6 Friction Head Loss

Pressure drop due to friction is a result of water flowing through a pipe and occurs between adjacent layers of water as well as between the water and the pipe inside wall. Therefore, pressure energy gets converted to kinetic energy which results in an energy loss in the form of heat. Therefore, the pressure acting on the upstream side of the pipe gets steadily decreased when the fluid is propagating toward the downstream side of the pipe. Pressure loss due to friction can also be described as head loss due to friction. The governing parameters are the flow rate, pipe length, pipe diameter, the roughness of the pipe inside wall, as well as water viscosity and specific gravity.[15, pp. 11].

To calculate the head loss due to friction, the Darcy-Weisbach equation can be utilized which describes the pressure loss due to friction when fluid flows through a pipe as shown in Equation (46).

$$h = f \frac{L}{D} \frac{V^2}{2g} \tag{46}$$

where:

h is the friction pressure loss [m]

f is the Darcy friction factor [-]

L is the pipe length [m]

D is the pipe inside diameter [m]

V is the average velocity [m/s]

g is the acceleration due to gravity [m/s^2]

Reformulating this equation in terms of flow rate leads to Equation (47), used to calculate the head loss due to friction.

$$H_{Lfriction} = \frac{f * L_{pipe}}{(2 * g * D_{pipe})} * \left(\frac{4 * q}{\pi * D_{pipe}^2}\right)^2 \quad (47)$$

where:

f is the Darcy friction factor [-]

L_{pipe} is the pipe length [m]

[12, pp. 29]

The Darcy friction factor must be determined in order to compute the head loss due to friction. If the flow is laminar, this component is determined just by the Reynolds number; however, in a turbulent environment, additional parameters are required. Several formulations are valid just for laminar or turbulent flow regimes, as well as smooth or totally turbulent flows, but they do not cover the entire spectrum. However, for applications in computer simulations, it is more convenient to use a single formula that covers the whole spectrum, laminar and turbulent, as well as the transition phase. Equation (48) shows the proposed formula after Cheng.

$$\mathrm{f} = \frac{1}{\left(\frac{Re}{64}\right)^a * \left(1.8 * \log\left(\frac{Re}{6.8}\right)\right)^{(2*(1-a)*b} * \left(2 * \log\left(\frac{3.7 * D_{pipe}}{\varepsilon_{pipe}}\right)\right)^{2*(1-a)*(1-b)}} \quad (48)$$

where:

Re is the Reynolds number [-]

ε_{pipe} absolute pipe roughness [m]

Parameters a and b are given as

$$a = \frac{1}{1 + \left(\frac{Re}{2720}\right)^9} \tag{49}$$

$$b = \frac{1}{1 + \left(\frac{Re}{160 * \frac{D_{pipe}}{\varepsilon_{pipe}}}\right)^2} \tag{50}$$

[16, pp. 1-3]

3.3.7 System Head

The system head is calculated according to Equation (51) and includes all hydraulic losses occurring in the hydraulic subsystem such as the static head, the velocity head, the local head losses, and the friction head losses.

$$H_{sys} = H_s + H_V + H_{Llocal} + H_{Lfriction} \tag{51}$$

[12, pp. 28]

Chapter 4

Matlab Simulink Model

Modeling allows representing a real-world application in a virtual environment and alteration of certain parameters under a variety of scenarios. Especially in the early stages of the design process of a new product, modeling and simulations provide benefits to increase the quality of the system design by reducing the number of errors that might occur along the implementation process especially if new hardware is yet not available. The model-based design offers fast and cost-efficient development of dynamic systems with the system model at the center of the workflow.

Simulink is a software program that provides a block diagram environment in form of a graphical editor, customizable block library, and integrated solvers to model dynamic systems in a multidomain simulation. Due to its integration in MATLAB with the so-called Function block, it offers possibilities to incorporate algorithms from MATLAB into models as well as providing options to export simulation results to MATLAB for further analysis. In addition, Simulink offers a sophisticated library of predefined blocks to build and manage continuous-time and discrete-time systems. The simulation engine is designed such that it offers various options to solve ordinary differential equations in fixed-step or variable-step. With the implementation of scope blocks and display blocks, simulation results can be tracked in real-time and certain analysis tools provide options to refine the model architecture and increase simulation speed. [17, pp. 1, 2]

4.1 Simulink Block Description

The Constant block generates a constant value signal. It is either real or complex in the form of scalar, vector, or matrix

The Gain block is used to multiply the input value by a constant value with both being either a scalar, vector, or matrix

The Sum block adds or subtracts a scalar, vector, or matrix from the input value based on the option selected within the block signal parameters

The From block gets a signal from its corresponding Goto block that is used as an output signal. The data type of the input and output needs to be the same and there is no connection between these blocks

The Goto block is used to deliver the input to its corresponding From block as a real- or complex-valued signal or vector of any data type.

The Step block is used to change the value to two defined levels at a specified time with the output signal being the initial value if the simulation time is less than the step time or the output signal being the final value for simulation times equal to or larger than the step time

The Manual Switch block is used to switch between two different inputs and pass it through to the output. The signal flow needs to be set before running the simulation

The Mux block is used for a simplified visual appearance. It combines inputs of the same data type and complexity into a single vector output

The Demux block is used for a vector input signal to be extracted as individual signals while the output ports are ordered from top to bottom

The Scope block displays a time-domain signal graphically

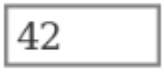

The Display block shows a signal value during simulation in real-time

The MATLAB Function block is used to execute a MATLAB function inside the Simulink simulation

The Integrator block is a dynamic system with one state. Input signals are solved by numerical approximation methods with respect to time and the output is the value of the integral of the input signal

[18]

4.2 Simulation Setup

The Simulink model of the digital twin is designed such that all input parameters are defined in a so-called initialization file. The purpose of this initialization file is to give an overview of all parameters needed to execute the simulation and the possibility to alter certain parameters without searching for them in a deeper layer of the Simulink model. These initialization parameters include motor-specific variables such as inductances, resistivities, and pole pairs, the drag coefficient, and motor inertia, the parameters for both polynomial pump functions as well as input parameters for the hydraulic subsystem:

```
clear all; close all; clc

Us = 440;           %supply voltage [V]
fs = 50;            %frequency of supply voltage [Hz]
Lm = 0.5;           %mutual inductance coupling stator and rotor [H]
Lr = 0.03;          %rotor winding leakage inductance [H]
Ls = 0.03;          %stator winding leakage inductance [H]
Rs = 6;             %stator winding series resistance [ohm]
Rr = 6;             %rotor winding resistance [ohm]
P = 1;              %pole pairs
%D = 0.003;          %total friction/drag [Nm/rad*s^-1]
D = 0.062;
%J = 0.02;           %rotor inertia [kg*m^2]
J = 0.8;
TL = 10;            %load torque
%plot Pump Curve    plot(out.Flow_Rate,out.Head)
%head polynomial function
a = 8.12931531923439e-05;
b= -1.02338324885707;
c = 8.12931531923439e-05;
%pump torque polynomial function
at = -5804100.9475758;
bt = 142.668344435107;
ct = 0.000525852859880895;
%Pipe Model
Dpipe = 0.0508;     %pipe diameter [m]
piperoughness = 0.015; %roughness of pipe [m]
Lpipe = 12.9;       %pipe length [m]
A = pi*Dpipe^2/4;   %Pipe area [m^2]
%valve 1 (Globe Valve)
d11 = 1*Dpipe;    %fraction of valve 1 open with regards to pipe
d12 = 1*Dpipe;
step_time_1 = 0;  %[s]
%valve 2 (Globe Valve)
d21 = 1*Dpipe;       %fraction of valve 2 open with regards to pipe
d22 = 1*Dpipe;
step_time_2 = 0;  %[s]
%height difference tank pump
h2 = 2.06;          %pump intake height [m]
h1 = 0.92;          %tank outlet height [m]
g = 9.81;           %acceleration due to gravity [m/s^2]
%Head losses
Kmp = 0.5;          %sudden contraction between tank - pipe [-]
Kpt = 0.3;          %change in pipe geometry [-]
%fluid parameters
rohwater = 997.05;  %water density [kg/m^3]
waterdynvis = 0.001;%water dynamic viscosity [Pa*s]
```

Furthermore, the simulation is separated into seven different subsystems (Figure 17) that are connected following their relationship based on the mathematical formulations. These subsystems are the 3-phase power supply (yellow), the motor speed control (dark green), the Park transformation (purple), the electrical subsystem (dark blue), the electrical to mechanical subsystem (grey), the ESP subsystem (light blue), and the hydraulic subsystem (light green).

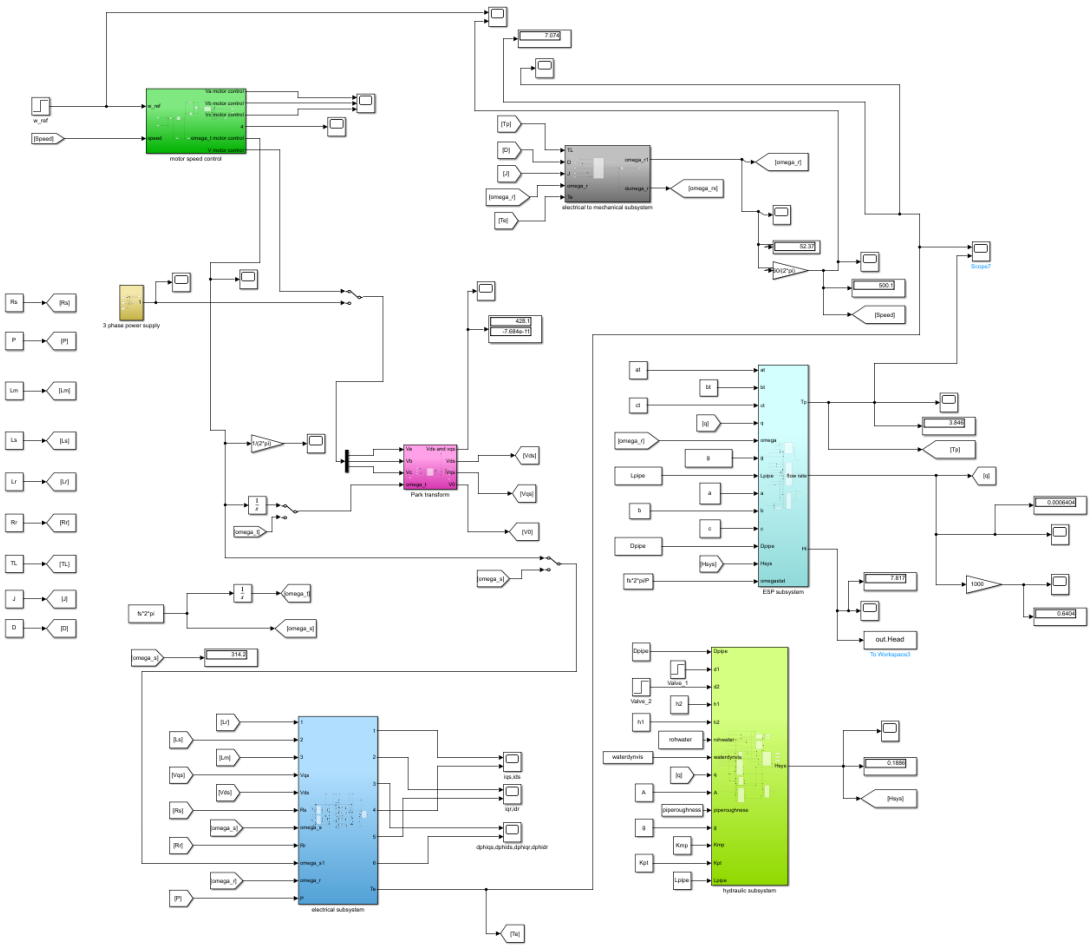

Figure 17: MATLAB Simulink Model Overview

4.2.1 Subsystem 3-Phase Power Supply

The 3-phase power supply subsystem generates a 3-phase voltage output where the amplitude of the voltage U_s and the corresponding frequency f_s are defined in the initialization file. The internals of this subsystem is shown in Figure 18 where V_a, V_b and V_c are the three voltages with a 120 [°] phase shift to each other.

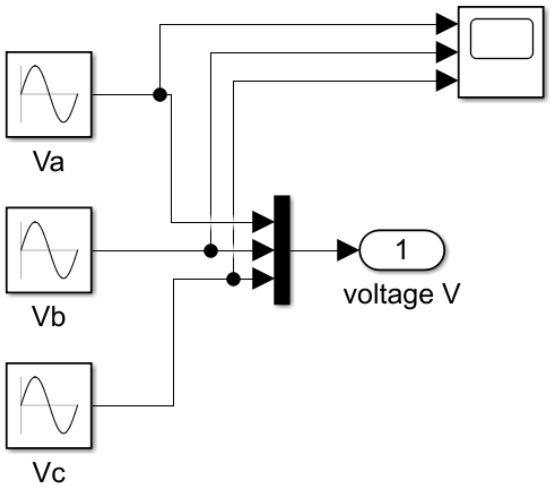

Figure 18: Subsystem 3-Phase Power Supply

4.2.2 Subsystem Motor Speed Control

The motor speed control subsystem (Figure 19) uses a reference speed ω_ref that is predefined and the actual motor speed as input values. The speed control is based on the principle of constant Volt/Hertz control, also called scalar control. The stator waveforms have a sinusoidal shape, and the frequency and magnitude can be altered. In addition, the control system does have a built-in feedback loop that compares the actual speed signal from the motor with the reference speed signal. This is realized with a PI-controller that performs proportional and integral control action so that the actual motor speed matches the reference speed. In addition, this subsystem is designed such that the voltages and frequency are calculated based on the induction motor dynamics with the individual voltages V_a, V_b and V_c as output.

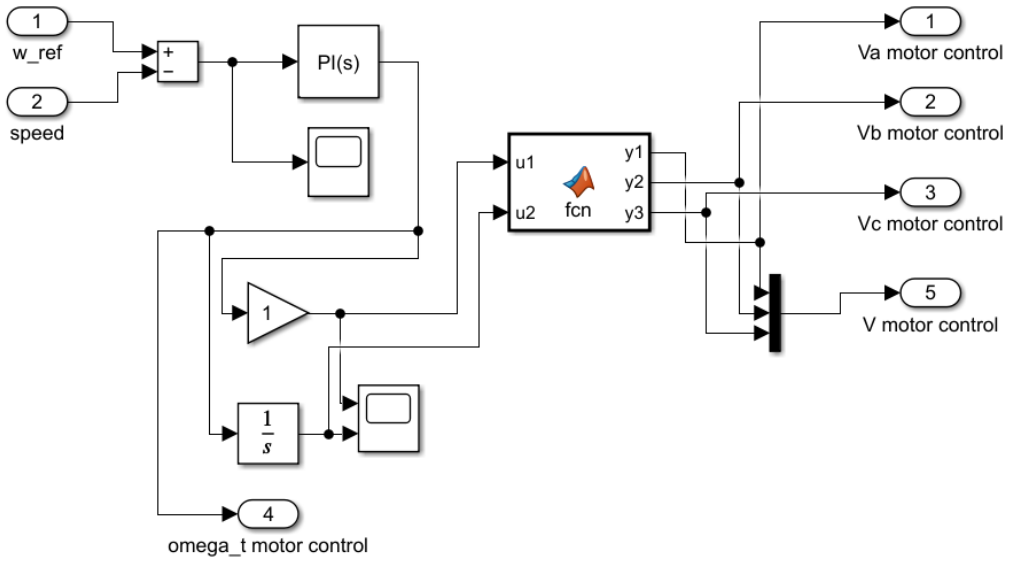

Figure 19: Subsystem Motor Speed Control

The Matlab function block for this subsystem is given as:

```
function [y1,y2,y3] = fcn(u1,u2)
y1 = u1*sin(u2);
y2 = u1*sin(u2+4*pi/3);
y3 = u1*sin(u2+2*pi/3);
```

4.2.3 Subsystem Park Transform

The Park transform subsystems (Figure 20) input parameters are the voltages V_a, V_b and V_c , and the angular velocity $omega\_t$. The output of this subsystem are the 2-phase system stator voltages V_{ds} and V_{qs}.

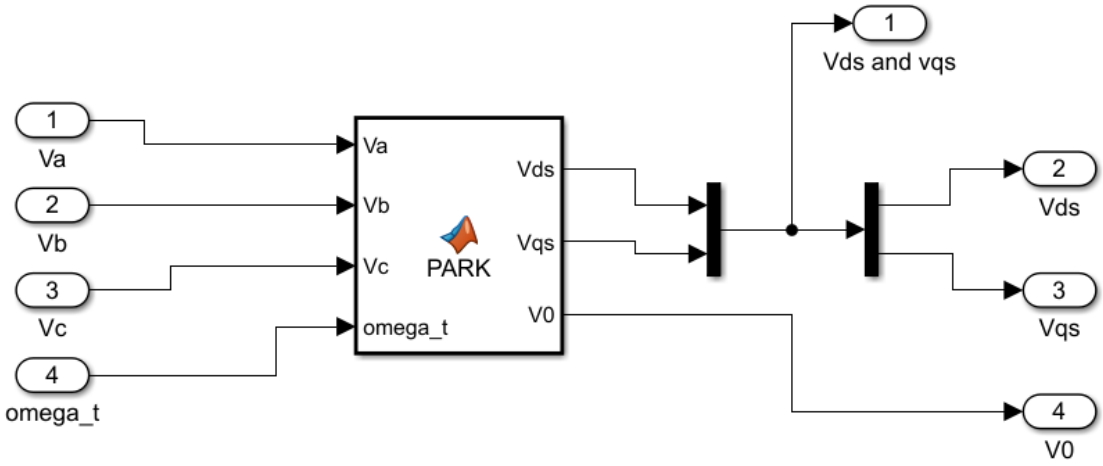

Figure 20: Subsystem Park Transform

The Matlab function block of this subsystem contains the mathematical formulations according to Equation (1) as follows:

```
function [Vds,Vqs,V0] = PARK(Va,Vb,Vc,omega_t)
Vds = 2/3*(Va*sin(omega_t)+Vb*sin(omega_t-2*pi/3)+Vc*sin(omega_t+2*pi/3));
Vqs = 2/3*(Va*cos(omega_t)+Vb*cos(omega_t-2*pi/3)+Vc*cos(omega_t+2*pi/3));
V0 = 1/3*(Va+Vb+Vc);
```

4.2.4 Electrical Subsystem

The electrical subsystem is split into four components. Two Matlab functions describe the stator and rotor electromagnetic fluxes (blue and green respectively) one that describes the electromagnetic torque (orange), as well as another subsystem for the stator and rotor currents (yellow) as shown in Figure 21. The input of the electrical subsystem are motor specific parameters from the initialization file as well as the voltages V_{ds} and V_{qs} from the Park transform subsystem.

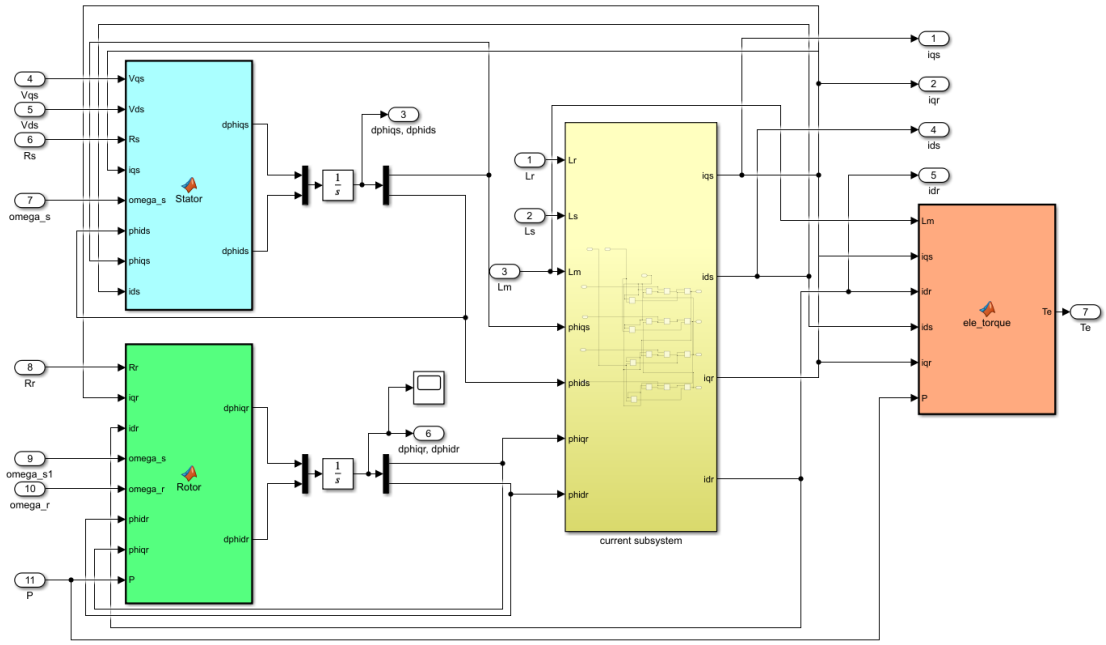

Figure 21: Electrical Subsystem

The Matlab function of the stator for calculating the electromagnetic fluxes of the q-axis $dphiqs$ and d-axis $dphids$ is based on Equations (3),(4) as follows:

```
function [dphiqs,dphids] = Stator(Vqs,Vds,Rs,iqs,omega_s,phids,phiqs,ids)
dphiqs = Vqs-Rs*iqs+omega_s*phids;
dphids = Vds-Rs*ids-omega_s*phiqs;
```

Similarly, the Matlab function of the rotor electromagnetic fluxes for the q- axis $dphiqr$ and d-axis $dphidr$ based on Equations (5),(6) is:

```
function [dphiqr,dphidr] = Rotor(Rr,iqr,idr,omega_s,omega_r,phidr,phiqr,P)
dphiqr =  -Rr*iqr+(omega_s-P*omega_r)*phidr;
dphidr = -Rr*idr-(omega_s-P*omega_r)*phiqr;
```

The current subsystem is based on Equations (11)-(14) with the rotor currents iqr and idr as well as the stator currents iqs and ids as output, shown in Figure 22.

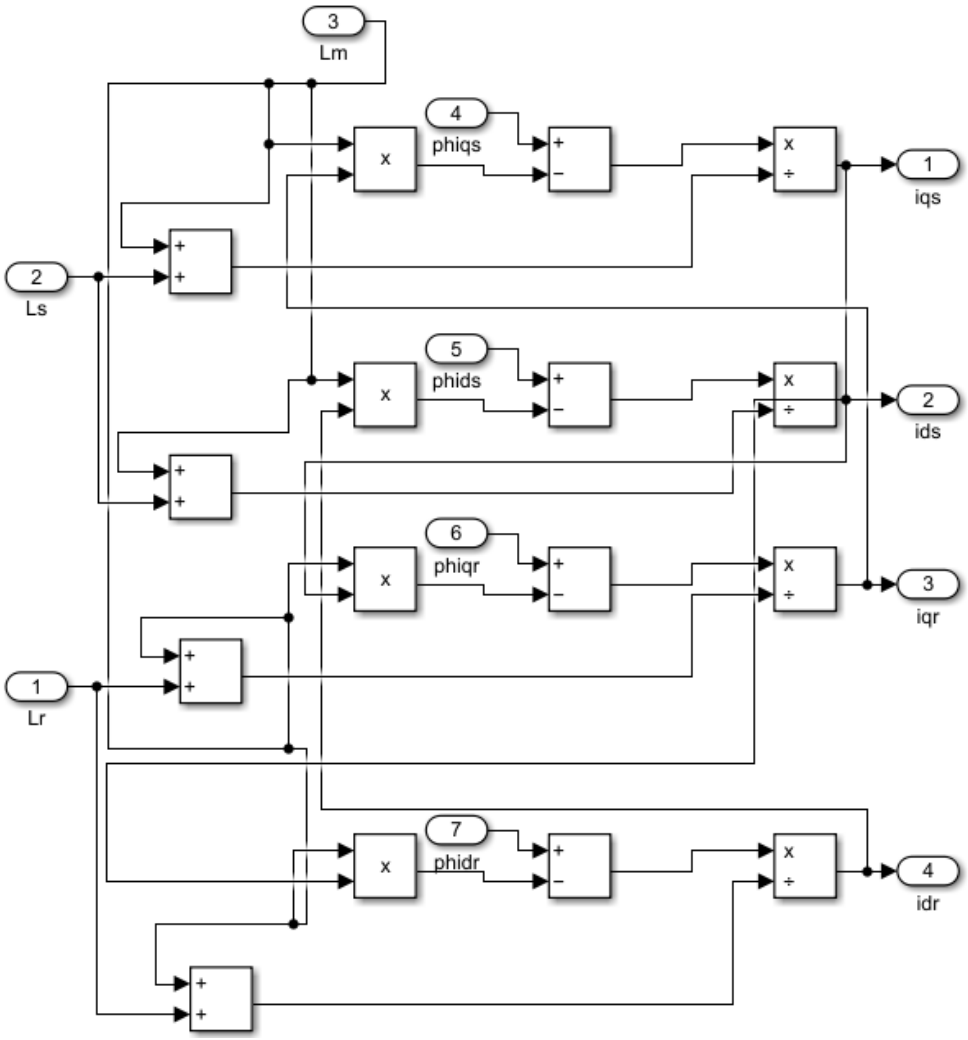

Figure 22: Current Subsystem

The Matlab function of the electromagnetic torque Te is based on Equation (15) and uses the output of the current subsystem as well as motor-specific parameters from the initialization file as input variables as follows:

```
function Te = ele_torque(Lm,iqs,idr,ids,iqr,P)
Te = P*(iqs*((ids+idr)*Lm)+ids*((iqs+iqr)*Lm));
```

4.2.5 Electrical to Mechanical Subsystem

This subsystem calculates the angular velocity $omega\_r$ of the motor shaft according to Equation (16). It is interdependent, meaning that the output angular velocity also functions as input for the next calculation step:

```
function domega_r = fcn(TL,D,J,omega_r,Te)
domega_r = (Te-TL-D*omega_r)/J;
```

4.2.6 Hydraulic Subsystem

The hydraulic subsystem is composed of eight Matlab functions describing the valve model (light green), static head (dark green), pipe velocity (light blue), velocity head (dark blue), local head losses (yellow), Cheng friction factor (purple), friction pressure losses (orange) and system head (red) as shown in Figure 23.

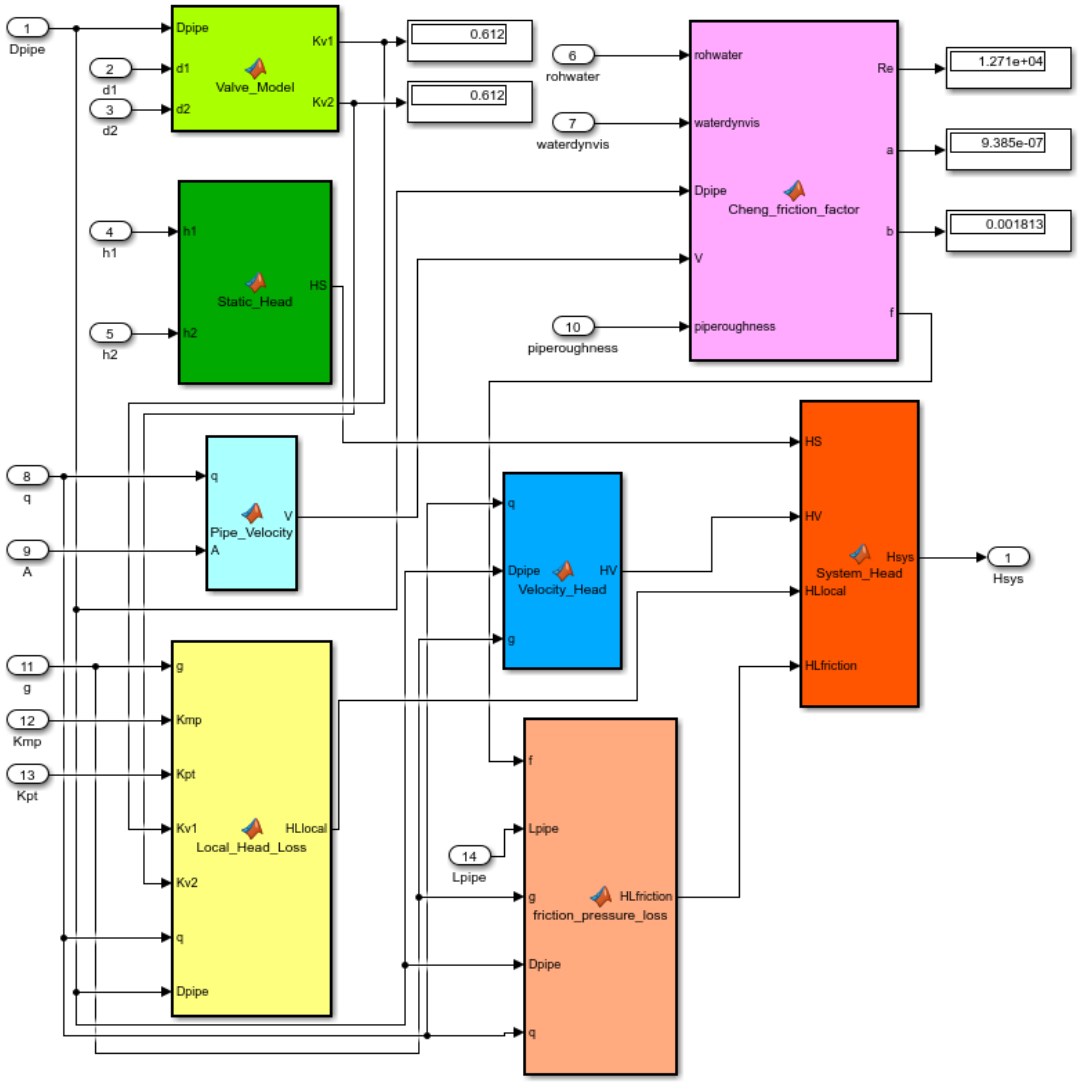

Figure 23: Hydraulic Subsystem

The Matlab function of the valve model is based on Equations (41)-(44). It is designed such that the flow through the valves can be adjusted from 0-100 [%] in terms of pipe diameter, with 0 [%] being fully closed and 100 [%] being fully open, expressed as $Kv1$ and $Kv2$:

```
function [Kv1,Kv2] = Valve_Model(Dpipe,d1,d2)
beta_valve1 = d1/Dpipe;
beta_valve2 = d2/Dpipe;
K = 340*0.0018;
Kv1 = (K+(0.5*(1-beta_valve1^2)+(1-beta_valve1^2)^2))/beta_valve1^4;
Kv2 = (K+(0.5*(1-beta_valve2^2)+(1-beta_valve2^2)^2))/beta_valve2^4;
```

The static head HS Matlab function is based on Equation (38) with the corresponding function given as:

```
function HS = Static_Head(h1,h2)
HS = h2-h1;
```

The pipe velocity V Matlab function calculates the fluid velocity inside the pipe based on $v = \frac{q}{A}$ and is given as:

```
function V = Pipe_Velocity(q,A)
V = q/A;
```

The local head loss $HLlocal$ Matlab function is based on Equation (40) with the corresponding function as:

```
function HLlocal = Local_Head_Loss(g,Kmp,Kpt,Kv1,Kv2,q,Dpipe)
HLlocal = 1/g*(Kmp+Kpt+Kv1+Kv2)*(4*q/(pi*Dpipe^2))^2;
```

The velocity head HV is calculated according to Equation (39) and the implementation as Matlab function is as follows:

```
function HV = Velocity_Head(q,Dpipe,g)
HV = (4*q/(pi*Dpipe^2))*1/(2*g);
```

The Cheng friction factor f is calculated based on Equations (48)-(50) with the corresponding Matlab function given as:

```
function [Re,a,b,f] = Cheng_friction_factor(rohwater,waterdynvis,Dpipe,V,piperoughness)
%Reynolds number [-]
Re = rohwater/waterdynvis*Dpipe*V;
%Chenga
a = 1/(1+(Re/2720)^9);
%Chengb
b = 1/(1+(Re/(160*Dpipe/piperoughness))^2);
```

```
%Cheng 1/f
x               =               max(min(((Re/64)^a*(1.8*log(Re/6.8))^(2*(1-
a)*b)*(2*log(3.7*Dpipe/piperoughness))^(2*(1-a)*(1-b))),1),0);
%Cheng friction factor f
f = 1/x;
```

The friction pressure loss $HLfriction$ based on Equation (47) implemented as Matlab function is as follows:

```
function HLfriction = friction_pressure_loss(f,Lpipe,g,Dpipe,q)
HLfriction = f*Lpipe/(2*g*Dpipe)*(4*q/(pi*Dpipe^2))^2;
```

The system head $Hsys$ Matlab function gets input parameters from the static head Matlab function, the velocity head Matlab function, the local head loss Matlab function, and the friction pressure loss Matlab function. It is based on Equation (51) and given by the corresponding Matlab function as:

```
function Hsys = System_Head(HS,HV,HLlocal,HLfriction)
Hsys = HS+HV+HLlocal+HLfriction;
```

4.2.7 ESP Subsystem

The ESP subsystem (Figure 24) includes three Matlab functions, the pump torque load (light blue), the pump head (orange), and the flowrate (yellow). The output of this system is the pump torque load Tp, the pump head Hi, and the flowrate $qout$. The calculated flowrate also functions as input to this subsystem for the subsequent iteration step, meaning that the subsystem is interdependent.

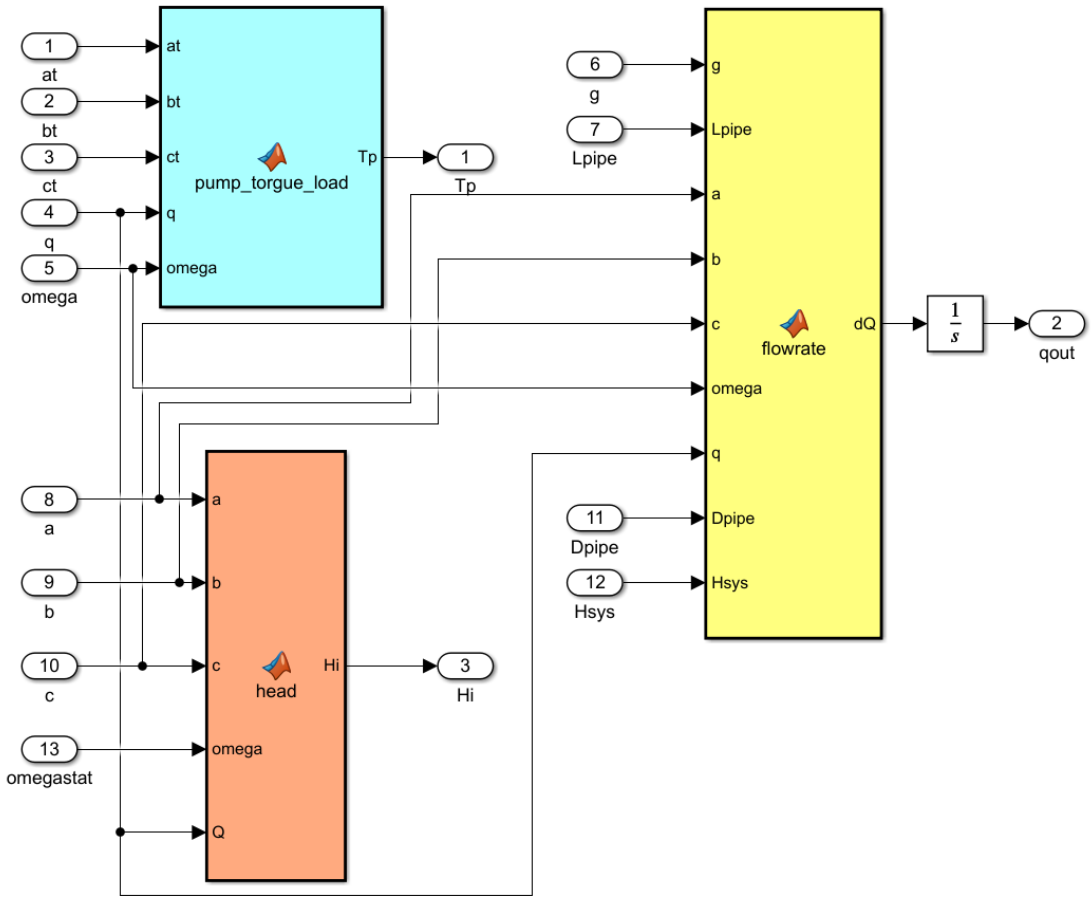

Figure 24: ESP Subsystem

The torque load of the pump Tp is given by the Matlab function according to Equation (31):

```
function Tp = pump_torgue_load(at,bt,ct,q,omega)
Tp = at*q^2+bt*q*omega+ct*omega^2;
```

The pump head Hi Matlab function block is based on the pump head polynomial function formulated by Equation (28):

```
function Hi = head(a,b,c,omega,Q)
Hi = a*omega^2+b*omega*Q+c*Q^2;
```

The flowrate Matlab function output is the pump flow rate based on the mathematical formulation given by Equation (37):

```
function dQ = flowrate(g, Lpipe, a, b, c, omega, q, Dpipe, Hsys)
A = pi*Dpipe^2/4;
dQ = g*A/Lpipe*(a*omega^2+b*omega*q+c*q^2-Hsys);
```

Chapter 5

Model Validation and Results

A simulation is conducted over a runtime of 430 [s] with the solver configuration set to variable step size and relative tolerance of 1e-3. The static input parameters of the induction motor, the ESP, and the hydraulic subsystem are used as given in the initialization file, while the dynamic input parameters motor reference speed and the opening states of valve 1 and valve 2 are varied throughout the simulation. Table 1 shows the designated time steps where these parameters are changed with their corresponding values.

Table 1: Dynamic Input Parameter

Timestep [s]	Reference Speed [rpm]	Valve 1 [% open]	Valve 2 [% open]
0	2917	60	100
38	2917	65	90
105	2917	66	100
132	2917	80	100
167	3267	80	100
213	3167	80	100
262	3117	80	100
286	2517	80	100
325	1717	80	100
382	1717	60	100
410	1717	5	100

5.1 Model Validation

The MATLAB Simulink model is validated by comparing the simulated flow rate to the flow rate measured during a test run conducted at the ESP testing facility as shown in Figure 25. It is important to note that whenever the flow rate is modified by changing a valve state, the simulated flow rate responds almost instantaneously, resulting in a sharp rise in flow rate. This behavior can be seen at every change of valve state throughout the simulation with an example of valve opening presented in Figure 26 and valve closing presented in Figure 27. A change in motor speed has a more gradual effect on the simulated flow rate due to the adoption of ramp and saturation functions and therefore better reflects the real behavior of the measured flow rate. It occurs at every change in speed with an example of a speed increase shown in Figure 28 and speed reduction presented in Figure 29.

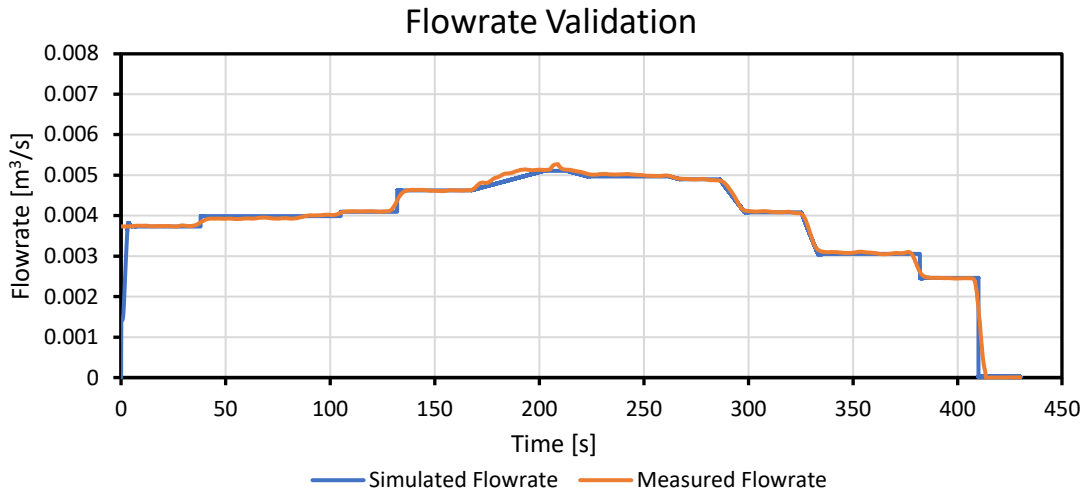

Figure 25: Simulated and Measured Flow Rate versus Time

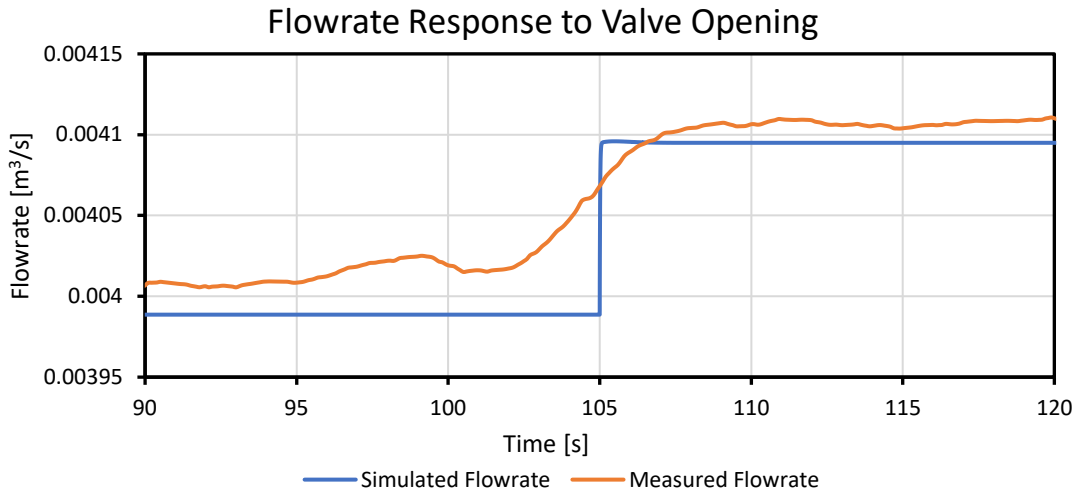

Figure 26: Flowrate Response to Valve Opening

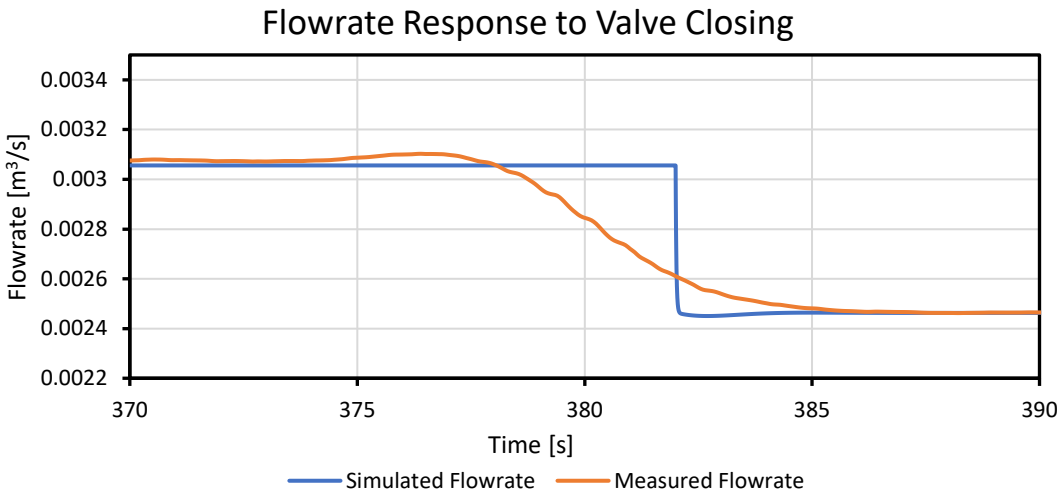

Figure 27: Flow Rate Response to Valve Closing

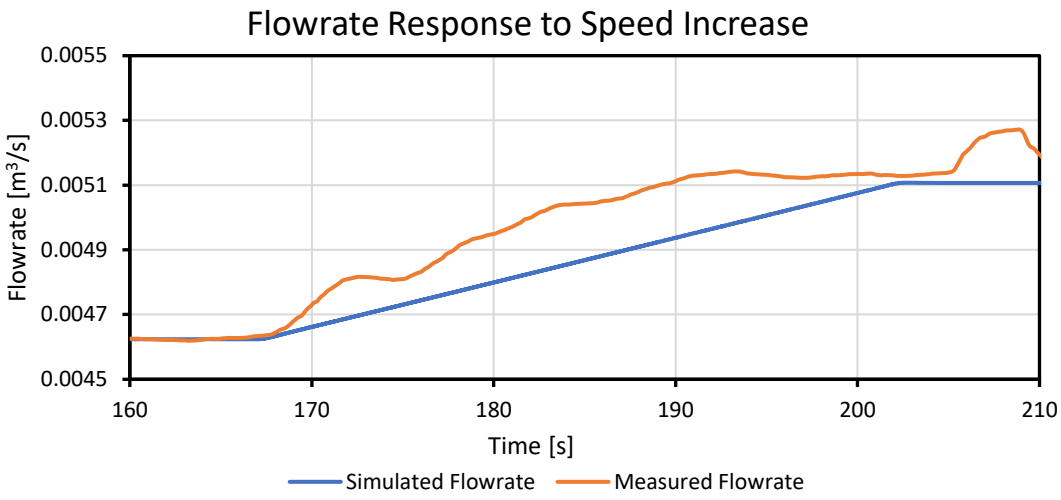

Figure 28: Flow Rate Response to Speed Increase

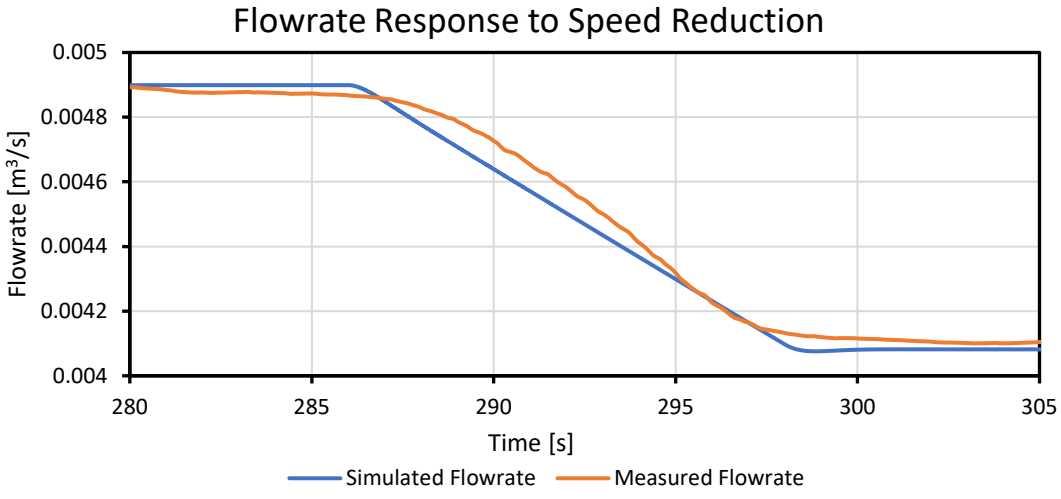

Figure 29: Flow Rate Response to Speed Reduction

In addition to the graphical evaluation of the difference between the simulated and measured flow rate, also the maximum and minimum difference, as well as the median, are determined Since the simulation is set to variable step size, MATLAB Simulink delivers data in irregular time steps while the measured flow rate from the ESP testing facility is captured in regular time steps of 0.1 [s]. Therefore, the simulation data are filtered and aligned to the measured data for a representative evaluation. Figure 30 shows the difference in terms of flow rate. Spikes are due to changes in valve state whereas changes in motor speed only lead to small differences.

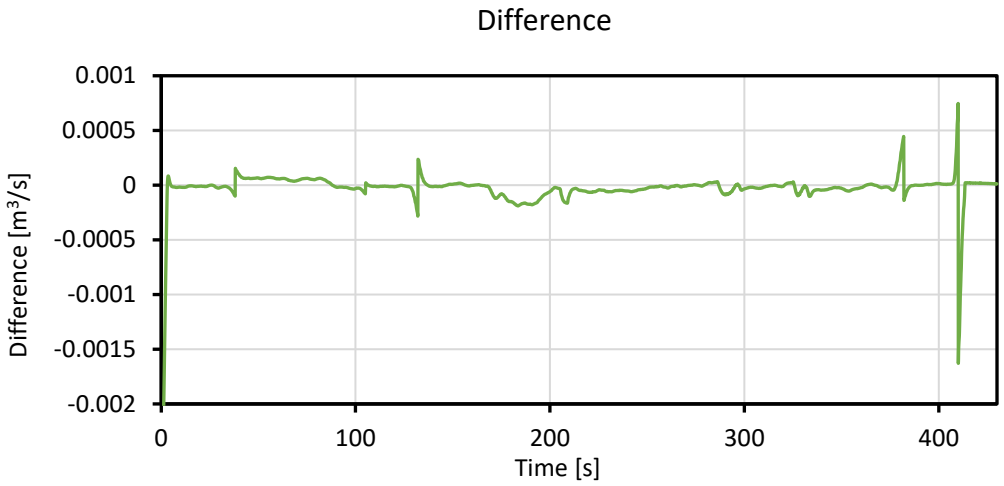

Figure 30: Flow Rate Difference

5.2 Results

In this section, additional outputs of the simulation such as motor speed, electromagnetic and load torque, as well as voltage response are discussed. These values are not validated with measured data from the ESP testing facility, however, they deliver more insights into the simulation and show dependencies between certain parameters.

5.2.1 Motor Speed

The motor speed of the simulation is shown in Figure 31. In the starting phase of the motor, the speed increases above the reference speed. This originates from the PI-controller of the motor control subsystem as it needs time to adjust to the reference speed. After a short duration, the actual motor speed equals the reference speed as shown in more detail in Figure 32.

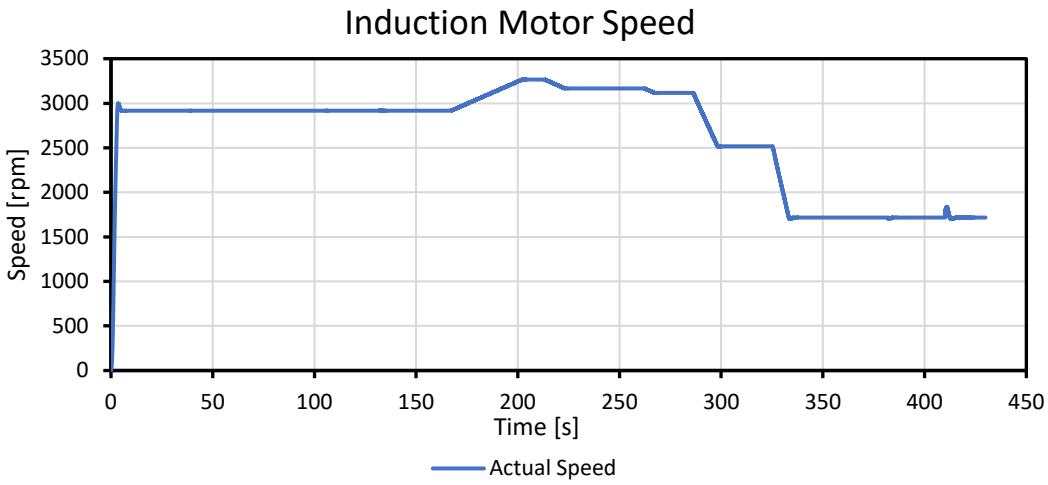

Figure 31: Motor Speed versus Time

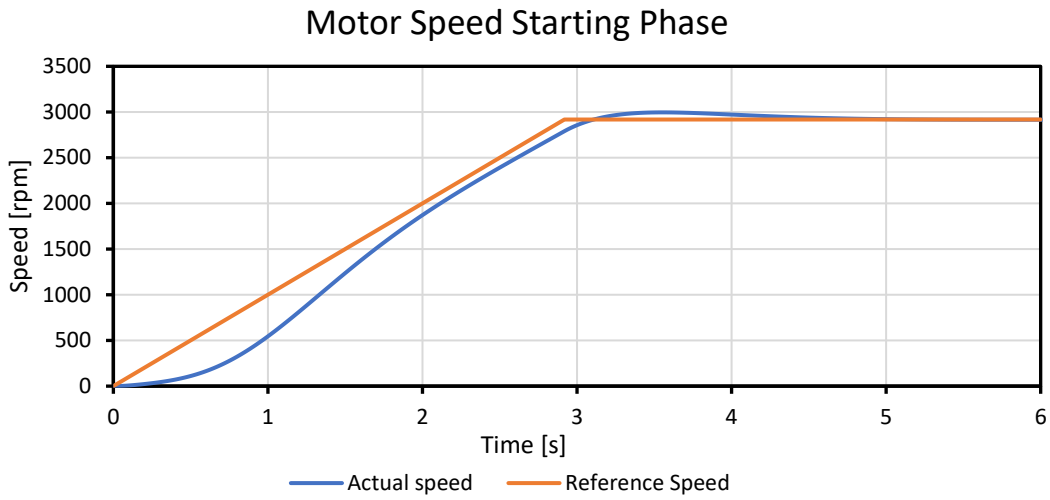

Figure 32: Motor Speed during Starting Phase

Another phenomenon can be observed whenever a valve state is changed as the motor responds with a small fluctuation in speed as a result of the motor reacting to a change in torque load. This behavior can be observed throughout every change of valve states for the entire simulation. A detailed example of valve opening is shown in Figure 33 and the response to valve closing is depicted in Figure 34.

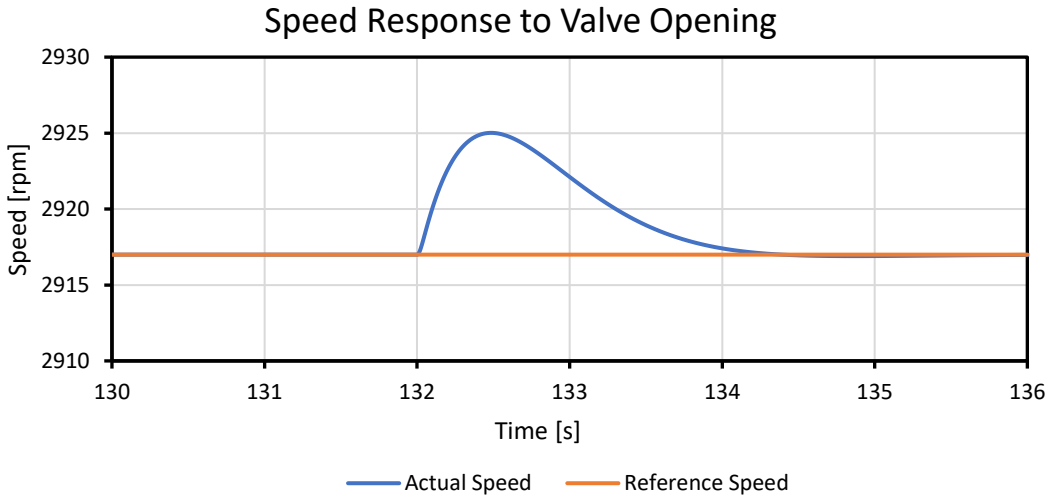

Figure 33: Motor Speed Response to Valve Opening

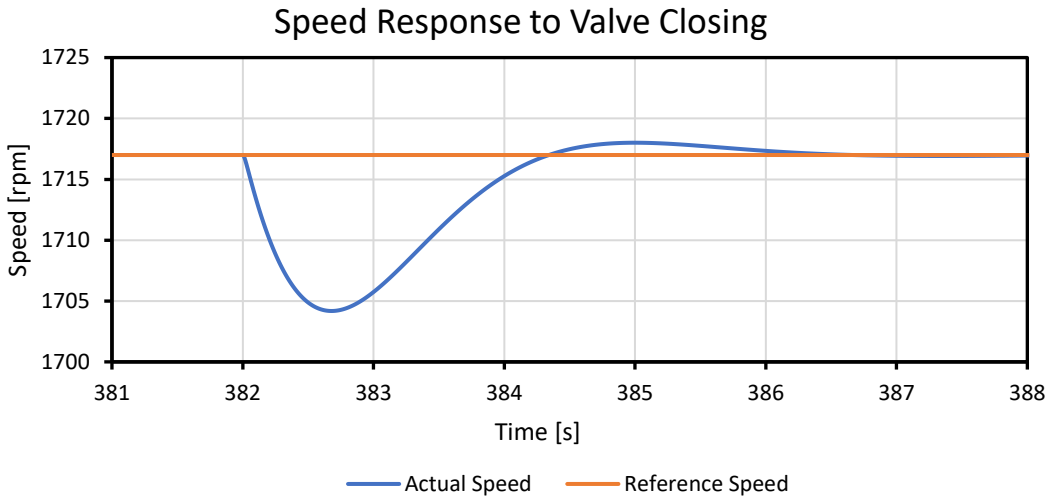

Figure 34: Motor Speed Response to Valve Closing

5.2.2 Electromagnetic Torque and Load Torque

Figure 35 depicts the electromagnetic torque produced by the induction motor and the load torque developed by the ESP. During the starting phase, a peak of the electromagnetic torque can be observed resulting from the inertia the motor needs to overcome. In addition, a small difference between both, the electromagnetic and the load torque, is caused by the dampening coefficient. Variations in motor speed and valve opening states cause changes in torque load.

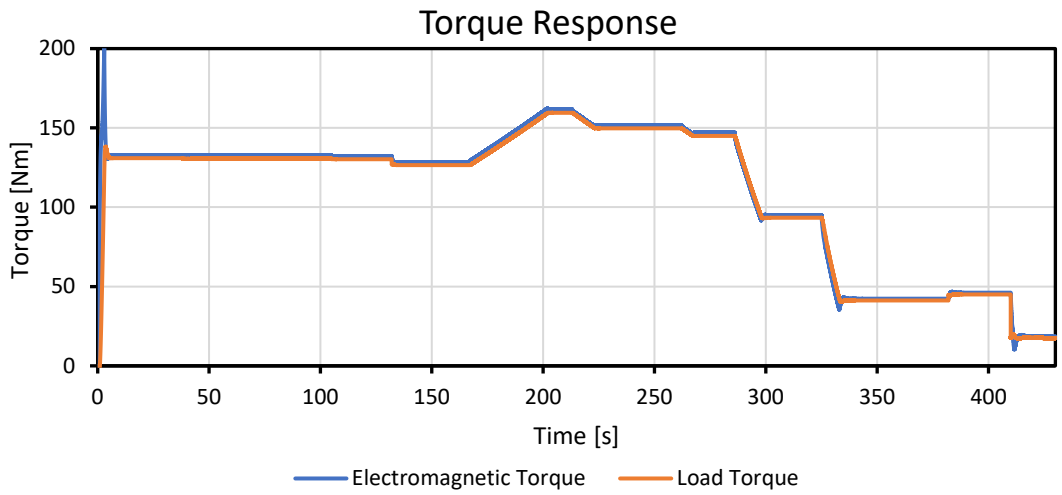

Figure 35: Electromagnetic Torque and Load Torque versus Time

When a valve opens the torque load decreases as there is less resistance to flow. As a result of the reduced load, the electromagnetic torque likewise reduces (Figure 36).

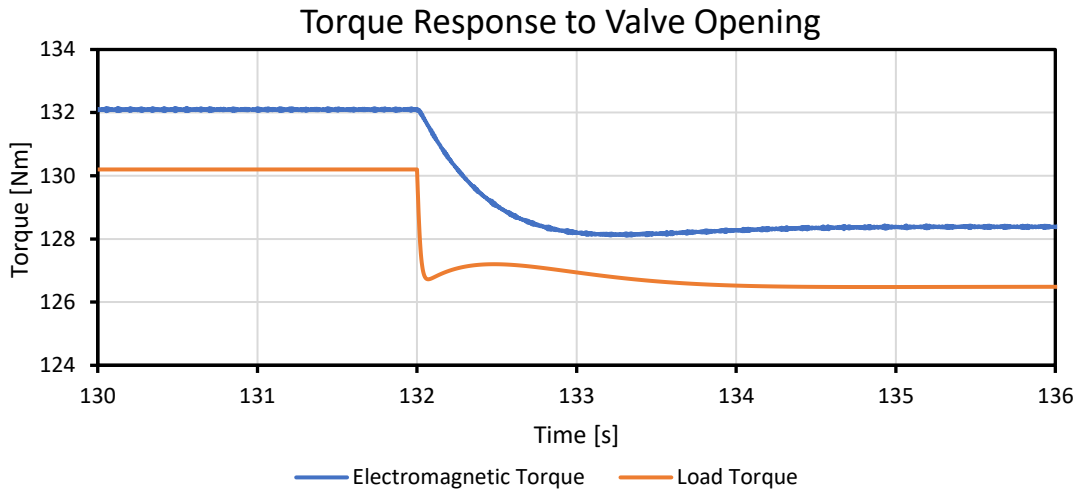

Figure 36: Torque Response to Valve Opening

When a valve reduces the flow path's diameter, the increased flow resistance results in a larger torque load, requiring the motor to provide more electromagnetic torque to maintain the system's reference speed (Figure 37).

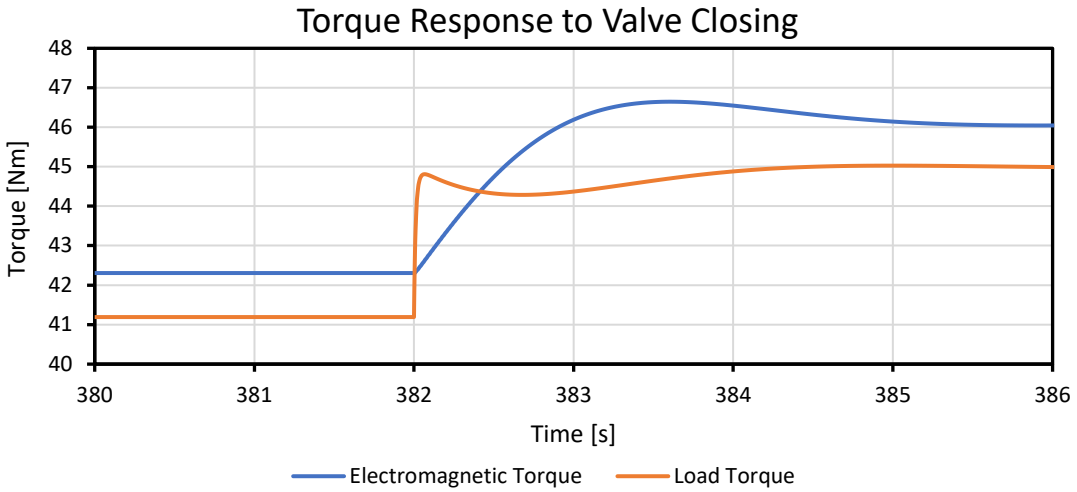

Figure 37: Torque Response to Valve Closing

Changes in motor speed follow the same concept. The torque load increases when the motor speed is raised, necessitating the motor to operate at a higher electromagnetic torque. At a speed reduction, the torque load decreases, and accordingly also the electromagnetic torque decreases until the motor runs at the new reference speed.

5.2.3 Voltage Response

The three-phase voltage output of the motor speed control is presented in Figure 38. Due to the high frequency and runtime of the simulation, the exact behavior of the individual voltage traces Va, Vb, and Vc can not be captured in detail, therefore, an exact evaluation of the voltage response is conducted with the converted two-phase voltage from the Park transform subsystem. However, it quantitatively shows the response of the three-phase voltage amplitude to changes in the motor speed as well as the impact of changes in valve states.

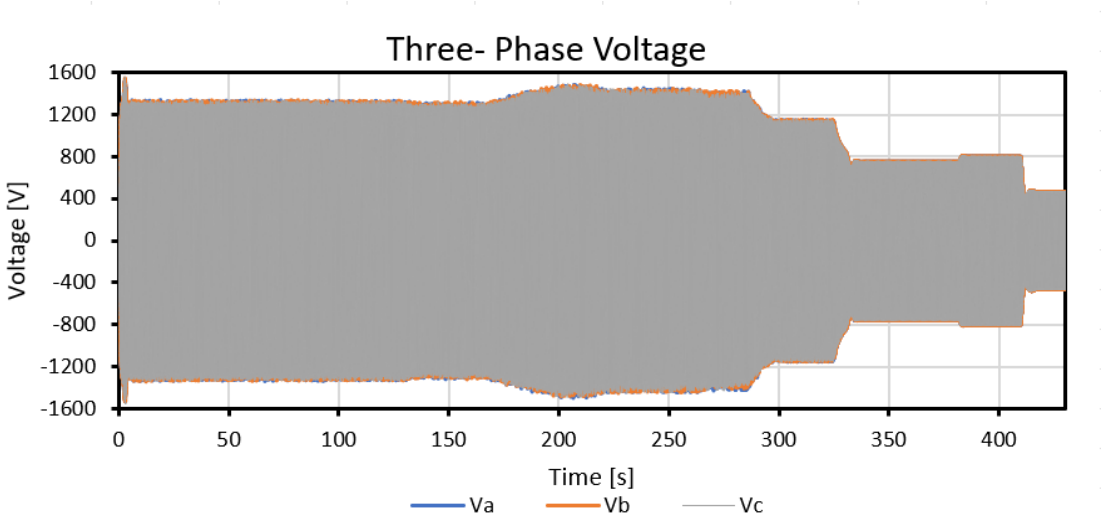

Figure 38: Three-Phase Voltage versus Time

Figure 39 shows the three-phase voltage in detail for the first 0.2 [s] of the simulation. It starts with a value of 0 [V] and then increases until enough voltage is provided so the system can operate at reference speed. Furthermore, it is shown that the voltage increase also leads to an increase in frequency which corresponds to the principle of the implemented induction motor scalar control.

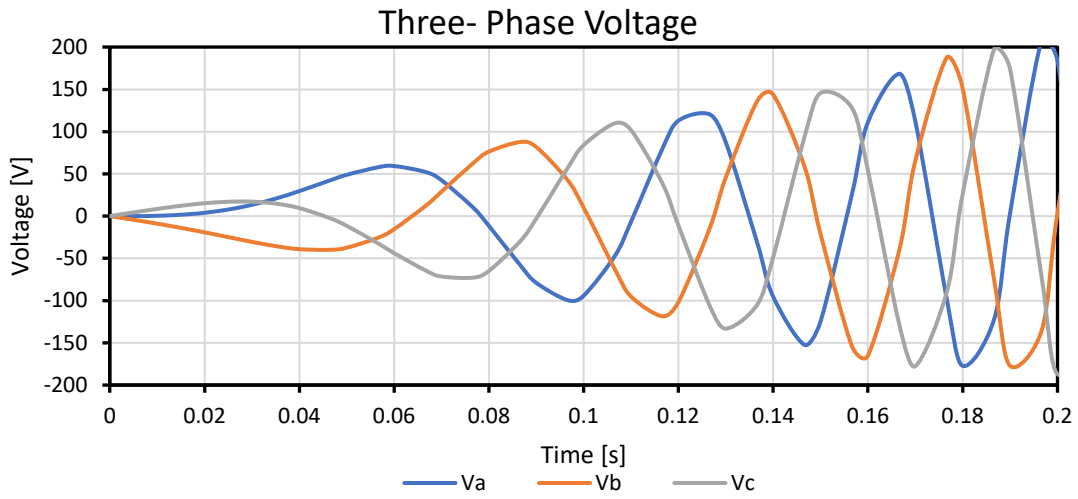

Figure 39: Three Phase Voltage during Starting Phase

The transformed three-phase voltage to a two-phase voltage in synchronous rotating reference frame is depicted in Figure 40. According to the Park transformation, the magnitude of the stator voltage in the quadrature axis Vqs is zero and the magnitude of the stator voltage in the direct axis Vds is equivalent to the amplitude of the three-phase voltage. Due to the high electromagnetic torque required by the motor to overcome initial inertia, a peak in voltage is observed at the start of the simulation. When the motor is running at reference speed, the voltage

lowers and remains constant in relation to the reference speed. Furthermore, the voltage responds to changes in reference speed and valve states according to the electromagnetic torque.

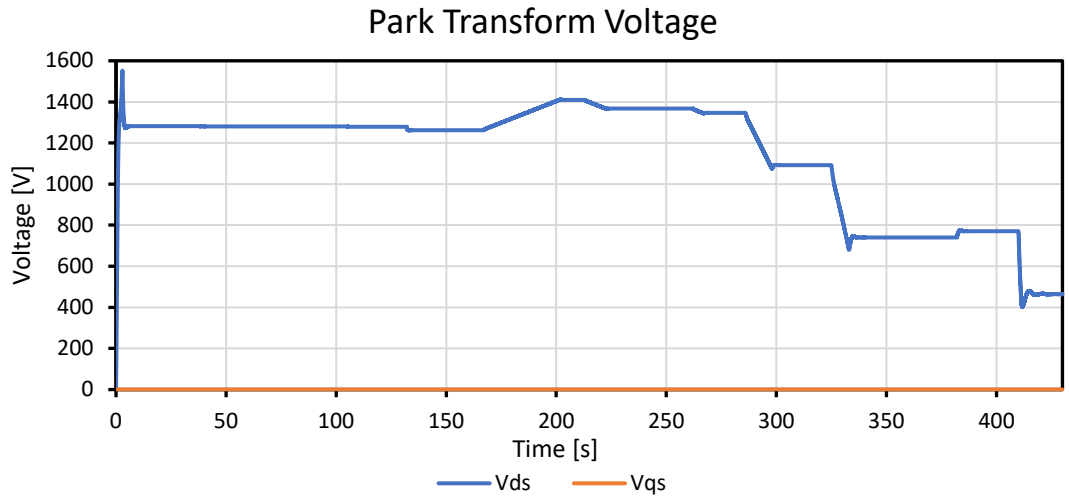

Figure 40: Two-Phase Voltage in Synchronous Rotating Reference Frame

When a valve opens, less electromagnetic torque is required to maintain the system operating at the specified reference speed since the resistance to flow gets reduced and thus, the motor control subsystem provides less voltage (Figure 41).

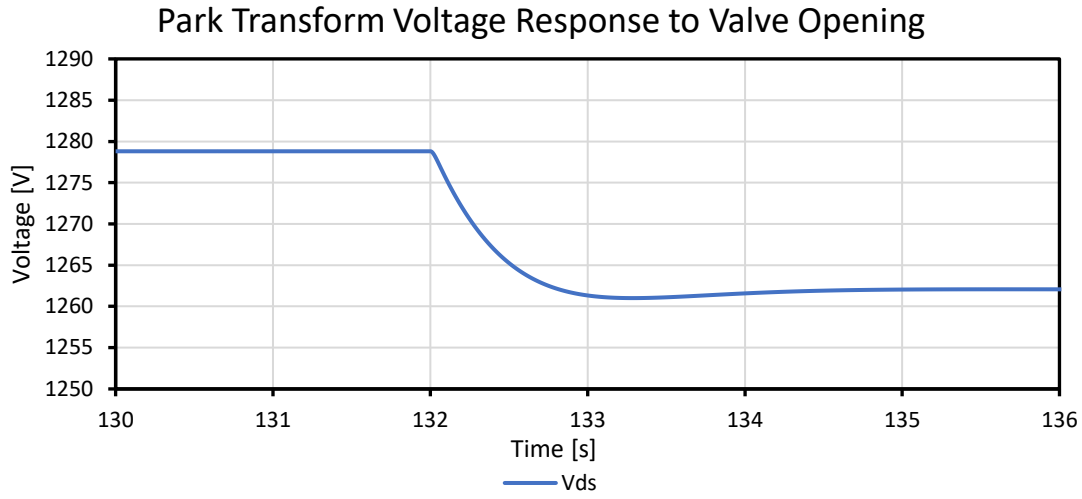

Figure 41: Two-Phase Voltage Response to Valve Opening

Valve shutting causes a greater resistance, requiring an increase in voltage from the motor control subsystem to maintain the specified reference speed (Figure 42).

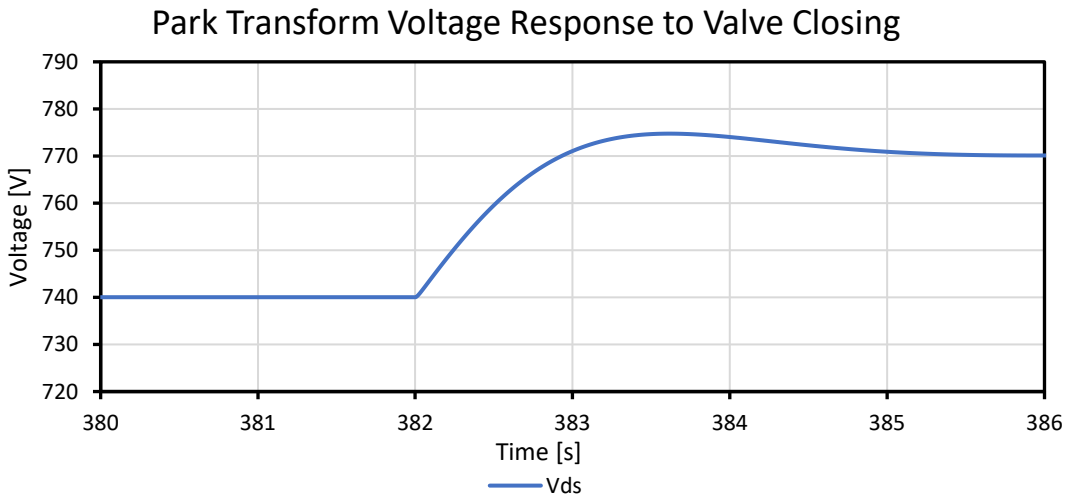

Figure 42: Two-Phase Voltage Response to Valve Closing

Similarly, higher electromagnetic torque is required to operate the system at a higher reference speed, hence more voltage is delivered, whereas a lower reference speed results in a voltage drop.

Chapter 6

Conclusion

6.1 Summary

Digital Twins provide great opportunities and potential for the oil and gas industry not only to increase production and optimize existing operating procedures but also to meet steadily rising requirements in terms of health, safety, and environment, and cope with strict regulatory compliances. Since the physical asset is linked to the digital twin, data exchange is possible and enables constant communication to monitor and control as well as optimize the physical counterpart. Future trends such as malfunctions or failures can be identified and prevented, and new production configurations can be tested and evaluated. However, a Digital Twin implementation does also bring challenges and risks. Employees for example need to undergo training to properly handle Digital Twins, a lack of standardization can reduce the Digital Twins' efficiency, and data ownership needs to be clarified as the protection of intellectual property rights is very important. Due to the constant cyber-physical connection, the system is very vulnerable to cyber criminality. Therefore the implementation of a proper cyber-security system is necessary.

The Digital Twin model of the ESP testing facility is realized in the software program MATLAB Simulink and consists of several subsystems. The induction motor is calculated in the Park frame, meaning that the three-phase system is transformed into an equivalent two-phase system in rotating reference frame. The pump is simulated with two polynomial functions, one for the head curve whose parameters are identified by utilizing the method of ordinary least squares, and the second for estimating the torque behavior with the parameters identified from a three-equation system. The hydraulic subsystem includes head losses due to friction, height difference, changes in pipe geometry, and velocity, as well as a model for two valves to adjust the flow rate. In addition, a motor control subsystem based on the principle of

scalar control offers the possibility to operate the system with a given reference speed where the built-in PI- controller adjusts the actual motor speed accordingly.

The proposed Digital Twin of the ESP testing facility delivers reasonable results and the model validation shows that it is capable of reproducing the measured flowrate with an overall small error margin.

6.2 Future Work

Although the model is very capable of reproducing the measured flow rate from the test run conducted at the ESP testing facility, other parameters such as voltage or electromagnetic torque are not validated. This is due to the lack of information on motor internal parameters that include resistivities, inductances, motor inertia, and dampening coefficient. It is also worth noting that the pump used for this simulation is randomly chosen from a pump catalog since pump-specific parameters such as performance curves were not available for the installed pump of the testing facility. Therefore, additional investigation is suggested in optimizing these parameters.

Another point is that the model is designed for simulating single-phase Newtonian fluids. Since the effects of non-Newtonian fluids, as well as two-phase and three-phase flow, may be of importance it is suggested to improve the model capable of accurately simulating them.

The valves are not spatially placed in the model compared to the pump facility where one valve is at the suction side of the ESP and the other one is located at the discharge side. Therefore, pressure readings are not included in the simulation.

Implementing all of the aforementioned suggestions can bring the Digital Twin model closer to its physical counterpart.

References

[1] Wanasinghe TR, Wroblewski L, Petersen BK*, et al.* Digital Twin for the Oil and Gas Industry: Overview, Research Trends, Opportunities, and Challenges. IEEE Access 2020; 8: 104175–97.

[2] Fuller A, Fan Z, Day C, Barlow C. Digital Twin: Enabling Technologies, Challenges and Open Research. IEEE Access 2020; 8: 108952–71.

[3] Mittal A, Slaughter A, Zonneveld P. Protecting the connected barrels: Cybersecurity for upstream oil and gas.

[4] Takács G. Electrical Submersible Pumps Manual: Design Operations and Maintenance (2nd Edition). Elsevier 2018.

[5] Takacs G. Sucker-Rod Pumping Handbook: Production Engineering Fundamentals and Long-Stroke Rod Pumping. Elsevier Science & Technology 2015.

[6] Green J. Induction Machine Model 2018.

[7] Surajit Chattopadhyay, Madhuchhanda Mitra, Samarjit Sengupta. Electric Power Quality (Power Systems).

[8] Park Transform: Implement abc to dq0 transform - Simulink; 2022 [cited 2022 May 19] Available from: URL: https://www.mathworks.com/help/physmod/sps/ref/parktransform.html.

[9] C. S. Kallesøe, Roozbeh Izadi-Zamanabadi, Henrik Rasmussen, V. Cocquempot. Model Based Fault Diagnosis in a Centrifugal Pump Application using Structural Analysis 2004.

[10] Steven J. Miller. The Method of Least Squares.

[11] Schlumberger. REDA Electric Submersible Pump Systems.

[12] Oulhiq R, Benjelloun K, Saad M, Kali Y, Deshayes L, editors. Dynamic Modeling and Simulation of a Slurry Mixing and Pumping Process: An Industrial Case. SCITEPRESS - Science and Technology Publications; 2019.

[13] Jirı Valtr. Mass Flow Estimation and Control in Pump Driven Hydronic Systems.

[14] Bell, Andrew, Caleb. Fittings pressure drop (fluids.fittings) — Fluids 1.0.21 documentation; 2022 [cited 2022 May 25] Available from: URL: https://fluids.readthedocs.io/fluids.fittings.html#valves.

[15] E. Shashi Menon. Piping Calculations Manual.

[16] Cheng N-S. Formulas for Friction Factor in Transitional Regimes. J. Hydraul. Eng. 2008; 134(9): 1357–62.

[17] The MathWorks, Inc. Simulink Getting Started Guide: MATLAB&SIMULINK.

[18] Block Libraries - MATLAB & Simulink; 2022 [cited 2022 May 25] Available from: URL: https://www.mathworks.com/help/simulink/block-libraries.html?s_tid=CRUX_lftnav.

List of Figures

List of Tables

Abbreviations

ESP	Electrical Sumbersible Pump
DT	Digital Twin
AI	Artificial Intelligence
3D	3-Dimensional
4D	4-Dimensional
CAD	Computer Aided Design
HSE	Health, Safety, and Environment
H-Q	Head- Flowrate
API	American Petroleum Institute
RP	Recommended Practice
AC	Alternating Current
DC	Direct Current
EMF	Electromotive Force
PI	Proportional Integral